Faculty of Science and Technology

Department of Physics and Technology

Forecasting Wind Turbine Production Losses due to Icing

Using the state-of-the-art IceLoss2.0 model together with numerical prediction models to create IceLossForecast.

Rikke Bjarnesen Andersen

Master's thesis in Energy, Climate and Environment EOM-3901

May 2023

Abstract

In order for wind energy producers to avoid the extra costs of inaccurate production estimates for the day-ahead energy market, precise forecasts of power production during the next day have to be made. For renewables such as wind energy, power production is particularly difficult to predict as it depends on the fluctuating wind speed. In addition, forecasting the power production in cold climates such as Norway is further complicated by the icing on wind turbine blades. The extra load on turbine blades due to icing leads to a decrease in power production.

Kjeller Vindteknikk has a state of the art model that estimates the production loss due to icing for new wind farms. This model uses historical weather data from the numerical weather prediction model WRF. To meet the interest from customers, Kjeller Vindteknikk wishes to further develop the icing model into IceLossForecast - An operational model providing production forecasts with icing loss for wind energy producers in cold climates. For this to work, the first step is to implement forecasting data into the IceLoss2.0 model and see if icing loss forecasts is comparable to historical IceLoss2.0 data. This is the objective of this thesis. Forecasting data from WRF forecast and the MetCoOp Ensemble Prediction model (MEPS) is implemented, and their results are compared to each other and to the current IceLoss2.0 estimates.

In this thesis MEPS and WRF forecasts has been implemented to IceLoss2.0 successfully. Results from one turbine at Kvitfjell Wind Farm has shown promising results both for WRF and MEPS that are comparable to the traditional IceLoss2.0 estimates with historical WRF data.

Acknowledgements

Contents

1 Introduction

1.1 Energy Market

The energy market in Norway is based on day-ahead trading of energy at the NordPool market. At the NordPool market energy producers and consumers deliver their offers and bids on energy (NordPool, n.d.). As energy needs to be used at the exact moment it is produced, there must be a balance between the energy produced and the energy consumed at all times (NVE, 2022a). An imbalance would change the power frequency which in turn can destroy equipment or in the worst case scenario a breakdown of the power grid (NVE, 2022b). To avoid such an imbalance, balancing power reserves are activated. In Norway, Statnett hold the task of maintaining the power balance within the market. When an activation of the power reserved due to an imbalance is necessary, an extra cost is added to the market actors that were responsible for the imbalance (Ferrieira, 2016).

Due to the cost of over- and underestimating the power production, creating accurate power production forecasts are of high importance for energy producers. For renewable energy sources such as wind energy, the prognostication is especially challenging due to the fluctuating wind resources (Gebrekiros & Doorman, 2014). To make it even more challenging, wind farms in cold climates such as Norway suffer from icing losses. That is, when ice builds up on the leading edge of the blade, the power production is reduced. Therefore, icing could potentially lead to a massive overestimation of the forecasted power production because it is not typically accounted for (Wallenius & Lehtomäki, 2015).

1.2 Previous Work

Kjeller Vindteknikk has developed a state-of-the-art IceLoss2.0 model that estimates the production icing loss for new wind farms. These estimates are based on historical data from the Numerical Weather and Research model WRF. The dataset spans from the year 2000 to the present date and is continuously updated in both past and present directions.

Kjeller Vindteknikk wishes to further develop this model so that icing forecast using IceLoss2.0 and two different weather models can be made and assist energy producers in their day-ahead power production estimates, as several customers have shown an interest for this after several large icing events in Finland during November 2022 (Lehtomäki, 2022).

As per today, a version of IceLossForecast is running operational on several wind farms in Finland. The owners of these wind farms are especially interested in forecasting the turbine

stops due to icing. This model has shown a hit rate of turbine stops between 22,9% and 41,0%, while the icing loss difference between the model and measurements, are between 0,2% and 1,2% (Kurppa et al., 2022). This model is based on forecasting data from the numerical weather prediction model WRF.

Although the icing loss results from the current IceLossForecast version are promising, it would be valuable to implement ensemble data as input to get a better understanding of how certain each forecast is. Ensemble data provides a set of forecasts instead of just one deterministic forecast. The different forecasts in the set are referred to as ensemble members. Each member contain some perturbations consistent with the uncertainties within the initial conditions (MetOffice, n.d.). This is done to account for some of the uncertainties within the forecast model.

During the fall of 2022 the author did a validation of the IceLoss2.0 model where model outputs were compared to SCADA data from eight turbines at Kvitfjell and Raudfjell Wind Farms (Andersen, 2022). The results were promising, especially for four of the turbines that had an active deicing system. Due to the success with icing loss estimates at these Wind Farms, the same location was chosen as a starting point when creating IceLossForecast with MEPS implementation. This work is based upon one turbine located at Kvitfjell Wind Farm. This turbine is located at a high elevation in the terrain, leaving it vulnerable to icing and a perfect candidate for testing IceLoss2.0 with forecasting models.

1.3 Objective

In this work, the main objective is to implement MEPS data into IceLoss2.0 to create an icing loss forecast that also can provide statistical measures like uncertainty of the forecasts. Together with the MEPS implementation, a similar WRF forecast implementation will be made as a reference to see how good the implementation is. These two forecasts will then be compared to the traditional IceLoss2.0 estimates with historical WRF data as input.

1.4 Paper Structure

This paper includes six chapters, Introduction, Theory, Method, Result and Discussion, Further Work and Conclusion. Their contents are described below.

The introduction Chapter 1 provides the necessary background information leading up to the objective of this work, as well as presenting the main objective.

Chapter 2 includes the relevant theory behind icing on structures such as turbine blades. Further, the numerical weather prediction models used in this work, WRF and HARMONIE-AROME are introduced. Lastly, the chapter covers the theory behind the IceLoss2.0 model. Note that some sections from this chapter are extracted from a project paper written by the author in the fall of 2022.

Chapter 3 covers the methods used in this work. This includes the preparation of input data and model set up. Along with a method used when analyzing the input data.

In Chapter 4 the resulting icing losses are presented. Time series of icing losses during the some chosen icing episode are plotted, as well as a snippet of the time series of power productions from all three IceLoss2.0 simulations with different input models. The results are discussed along the way as well.

Chapter 5 proposes further work that could be done to improve the results and make IceLoss Forecast operational.

Chapter 6 summarizes and concludes the main results from this work.

2 Theory

2.1 Icing on Wind Turbines

In cold climates icing on wind turbines is often a challenge. Ice buildup on turbine blades is mainly due to freezing rain or in-cloud icing. Freezing rain refers to subcooled air droplets that freeze when hitting a surface. In-cloud icing happens when the structure is covered in fog or cloud and the temperature is below 0 ∘C (Clausen, 2017). This blade ice buildup is removed in three ways, sublimation, melting and ice shedding (Nilsen, 2019).

There are several issues regarding icing on turbines. The most obvious one being loss of power. Ice loads on turbine blades increase the blades drag force while decreasing the blades lift force, causing the turbine to rotate slower and produce less (Lamraoui et al., 2014). Additionally, this imbalance and extra load also creates more stress on the blade and can impact the turbine fatigue reducing its lifetime. Another challenge with icing is the safety issue when ice shedding occurs. Ice shedding is when ice falls off the turbine blades. If this occurs while the blade is rotating, the ice could get thrown off at high speed and project far away from the turbine itself. This fallen or thrown ice are dangerous for people wandering the area.

One solution to the ice related issues is simply stopping the turbine when ice is detected. However, this does not solve the loss of production problem, and ice still may fall off the stand still turbine blades during melting (Ronsten et al., 2012). Another solution is blade heating, or deicing. Essentially the turbine blades are heated when icing occurs to prevent ice buildup so that the turbines can operate under icing conditions, but during heavy icing events the deicing system is not able to remove all the ice. Note that some of the produced energy will then be used for blade heating, or in some cases, the turbine would get energy from the grid to remove the ice. Therefore, deicing is only efficient in areas with sufficient icing loss, as a rule of thumb that is when the yearly energy production losses due to icing is above 1%.

2.2 Production Loss due to Icing

For wind turbines, there is a strong relation between the wind speed and the power produced. This relation is often referred to as the turbines power curve and is unique for each type of wind turbine generator. Figure 3-1 shows the power curve used from the wind farm investigated in this work. For wind turbines rotating, ice usually builds up at the leading edge of the turbine blades. Extra load on the blades increases the drag force and decreases the lift

force causing the turbines to rotate slower than they usually would at the current wind speed. If the turbines have an active deicing system, the blades would be heated to prevent ice from building. The turbine may then still rotate at its usual speed, but the production would still be reduced due to the heating. At significant icing events, the wind turbine generator would not produce as much as expected for the correlating wind speed. Hence, these events would appear under the power curve.

2.3 Kvitfjell/Raudfjell Wind Farm

Kvitfjell and Raudfjell WFs are located at the west coast of Northern Norway, in Troms County. The wind farms have 67 wind turbines in total. They are placed at elevations between 307.7 – 550.5 mas (meters above sea level). A validation report done by the author in Des 2022 showed that the icing loss for four turbines within this park located at different height was about 2-4% in Feb21-Feb22. Figure 2-1 below show wind roses for Kvitfjell and Raudfjell, which demonstrate the relationship between wind direction and strength, both in a general case, and in the case of ice events. As shown in the figure, the typical wind direction is from the South-Southeast. During icing the typical direction is from West, however it fluctuates from South-West to North-West. All the wind directions during icing are coming from offshore, suggesting that this air is warmer and holds more moisture.
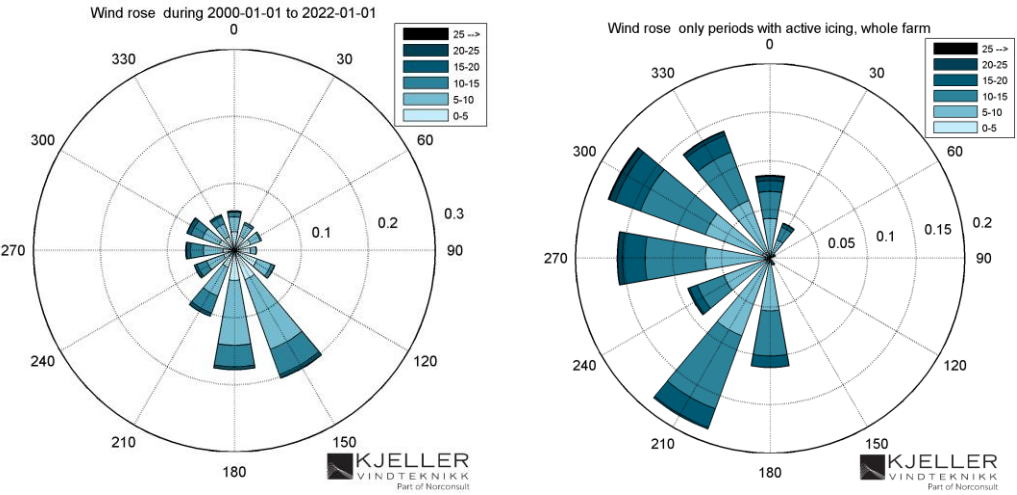

Figure 2-1: Wind roses of Kvitfjell/Raudfjell showing magnitude of wind speed and direction. Left: Average wind rose for the period 2000 – 2022. Right: Wind rose during only active periods of icing.

The turbines at Kvitfjell/Raudfjell wind farm are produced by Simens Gamesa, they have a hub height of 85m and rotor diameter of 130m. Each turbine can produce up to 4.2 MW of energy. Found from post-processing of SCADA data in previous work with validation of IceLoss2.0 that turbines had been adjusted up from 4.2 MW to 4.3 MW during the summer 2021. As an adjusted power curve had not been received until then, this was not accounted for. As this report compares forecast data with historical data made during that validation, the power curve is not adjusted for this case either. Table 1 summarizes the information about the wind turbines at Kvitfjell/Raudfjell wind park.

Table 1 Information about wind turbines at Kvitfjell/Raudfjell Wind Farm used in IceLoss2.0

Name	SWT-DD-130-4,2MW
Manufactory	Siemens
Hub height	85 m
Rotor diameter	130 m
Turbine elevation	307.7 – 550.5 mas
Maximum power	4.2 MW

2.4 Data

In this work, two different numerical weather prediction models have been used as input for IceLoss2.0. They are KVT Meso which uses the NWP model Weather Research and Forecast model (WRF), and MetCoOp Ensemble Prediction System (MEPS) which uses the HARMONIE-AROME model. Descriptions of each model are given in the following sections.

2.4.1 Weather Research and Forecast model (WRF)

WRF is a state-of-the-art Numerical Weather Prediction model designed for both atmospheric research and forecasting needs. It can produce simulations based on actual atmospheric conditions or idealized conditions (NCAR, 2023). It uses geographical and meteorological data as input. Inside of the chosen inner domain, it creates a box grid average based on the chosen resolution. The WRF hindcast simulations used as input for the IceLoss2.0 model covers the period from 2000-2022, while the WRF forecasting simulations each has a lead time of 49 hours. Both simulations have a horizontal resolution of 4 km. The WRF model runs with 32 vertical layers in total, with 4 layers below 200m. In addition, a 1 km resolution WRF simulation from 2005 are used to downscale the other simulation and make better wind descriptions (Liléo et al., 2013). The inner domain is called KVT-SWE06 and covers Norway and Sweden as shown in Figure 2-2 below depicts the domains of the WRF setup. The

historical WRF simulation is here on referred to as KVT Meso hindcast, while the WRF forecasting simulations are referred to as KVT Meso forecast.
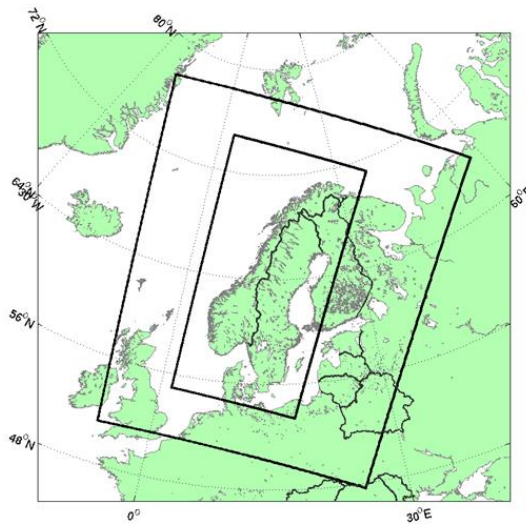
Figure 2-2: The outer and inner domain of KVT_SWE06 simulations (Kjeller Vindteknikk, n.d.-b)

For KVT Meso hindcast and forecast simulations on Kvitfjell/Raudfjell wind farm, the grid point marked in Figure 2-3 was used. This grid point is at a height of 253.6 mas for KVT Meso hindcast and 223.8 mas for KVT Meso forecast and is situated at the eastward end of Kvitfjell. This is the grid point closest to the parks both in elevation and distance, as the other points 4 km away from the one chosen were situated near sea level. Therefore, the chosen point was the most representative for this WF.
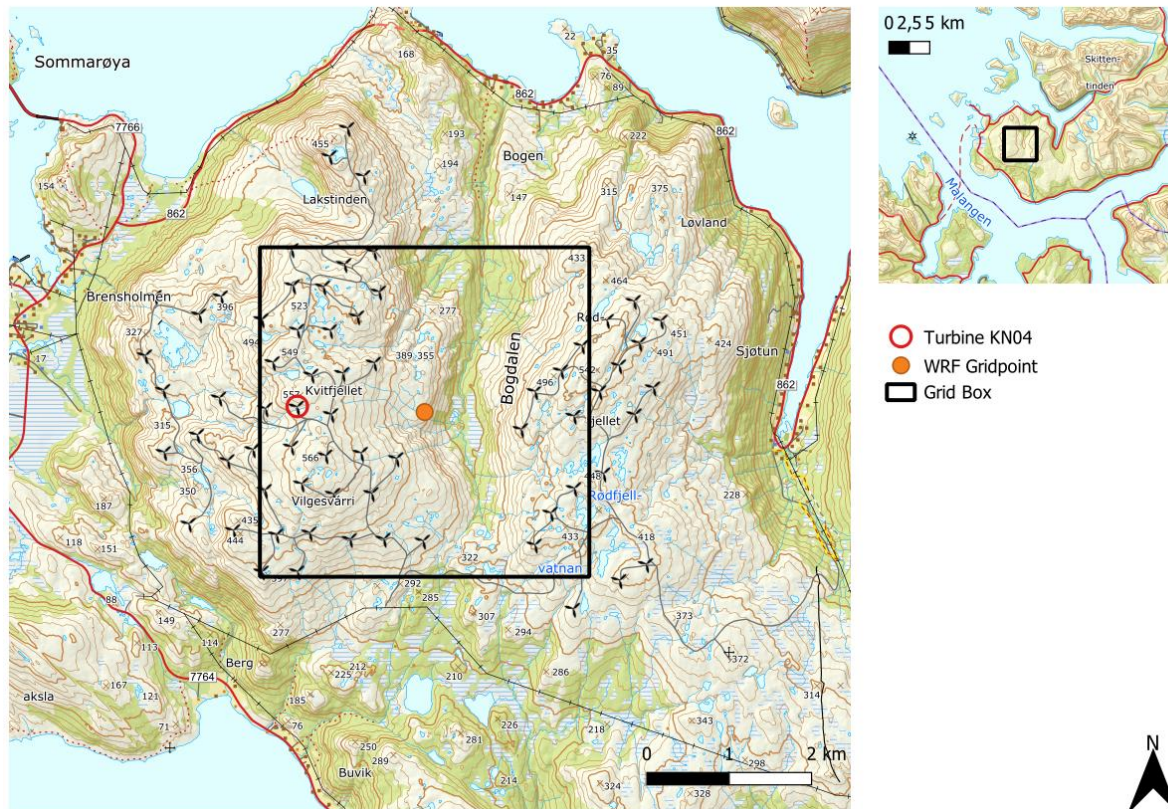
Figure 2-3 Map of Kvitfjell and Raudfjell WF, with the chosen WRF grid point marked. The grid point represents a box grid of size 4 km x 4 km. This point is situated as height 253.6 mas, according to model. Real terrain height at this point is 334.5 (Kartverket.no)

2.4.2 MetCoOp Ensemble Prediction System (MEPS)

The MetCoOp Ensemble prediction system (MEPS) is the ensemble realization of HARMONIE-AROME, producing 30 members. HARMONIE-AROME is a numerical weather prediction model used for operational short-range forecasting (Frogner et al., 2019). The domain used in these simulations covers Norway, Finland, Sweden and Denmark, as Figure 2-4 shows. The horizontal resolution is 2.5 km and the lead time for each simulation is 62 hours. Each day four simulations are made, at 00:00, 06:00, 12:00 and 18.00 (Forgner et al., 2019). The chosen grid point is in the middle of Kvitfjell wind park. Here the model elevation is 350 mas, while the real terrain height is 512 mas. Figure 2-5 shows the location of this grid point within the park. Usually, the preferred grid should not be above the lowest turbine in the park due to orographic lifting in IceLoss2.0 (section 2.5.1.2), but in this work only one turbine located at height 523 mas is studied. This turbine is marked as a red circle in Figure 2-5. Notice that it is located at the outline of the selected grid box area. The reason for choosing this grid point and the one on the other side of this outline is because this grid point

is closer in elevation to the selected turbine. The MEPS ensemble consists of 28 perturbations and 2 control members.

 The MEPS data is retrieved from an internal KVT server, originating from a Meteorological Institute service. Some of this data is available online, however some variables describing the liquid water content are not available. Therefore, the data available to IceLoss2.0 are only the ones from KVTs internal server.
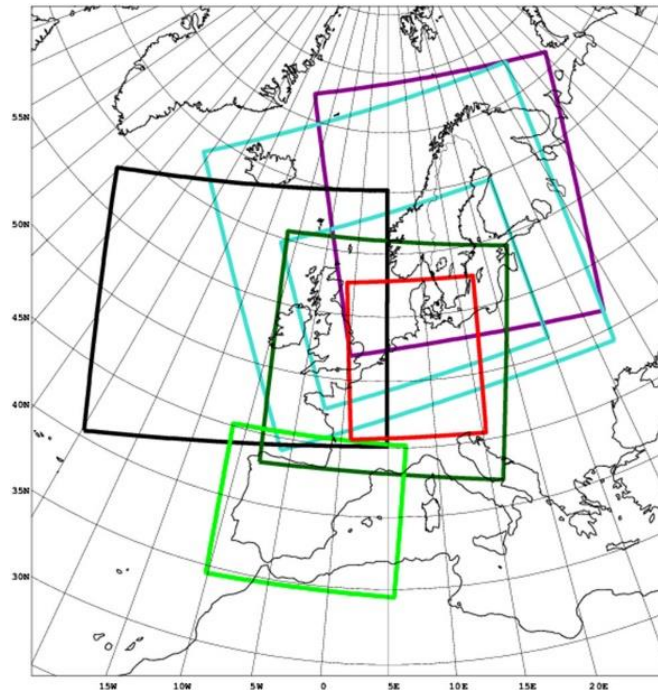
Figure 2-4 Schematic of Ensemble Prediction System domains using Harmonie-Arome. The purple square marks the domain used by cooperation with Finland, Norway and Sweden called MEPS or MetCoOp EPS. (Frogner et al., 2019)
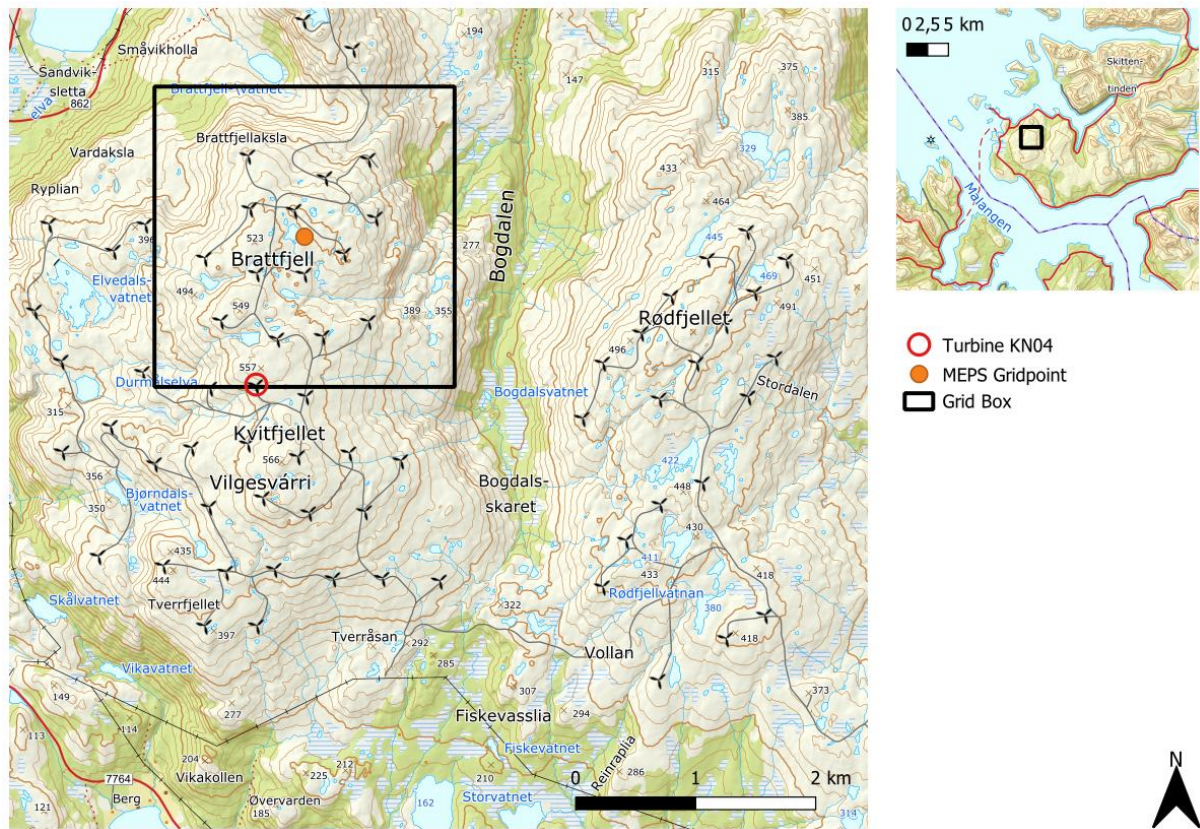
Figure 2-5 Map of Kvitfjell and Raudfjell WFs. The selected MEPS grid point is marked in orange surrounded by the outline of the 2.5 km x 2.5 km grid box it is representing. The red circle marks turbine KN04 investigated in this work. (Kartverket.no)

2.4.3 NWP Setup and Features

The table below sums up some of the model setup and features for the MEPS and WRF simulations used in this work.

Table 2: Model setup and features

| WRF hindcast, WRF forecast and MEPS model setup			
Model data	*KVT Meso hindcast*	*KVT Meso forecast*	*MEPS*
NWP model	*WRF*	*WRF*	*HARMONIE-AROME*
Members	*1*	*1*	*30*
Daily runs	*~*	*4*	*4*
Period	*2000-2022*	*48 hours*	*62 hours*
Spatial Resolution	*4 km x 4 km*	*4 km x 4 km*	*2.5 km x 2.5 km*
Temporal resolution	*1 hour*	*1 hour*	*1 hour*
Vertical resolution	*32*	*32*	*65*
Stored levels	*10*	*10*	*15*
Lateral boundary	*FNL*	*GFS*	*IFS*
Microphysics	*Thompson (8) (Thompson et al., 2004)*	*Thompson (8) (Thompson et al., 2004)*	*ICE3 (Taufour et al., 2019)*
Planetary Boundary Layer	*YSU (1) (Hong et al., 2006)*	*YSU (1) (Hong et al., 2006)*	*unknown*
Land surface physics	*5L-thermal (1)*	*5L-thermal (1)*	*SURFEX (Le Moigne, 2009)*
Surface layer	*MMS (1)*	*MMS (1)*	*unknown*
Radiation Scheme	*RRTMG*	*RRTMG*	*unknown*
Initial and boundary perturbations	*~*	*~*	SLAF, surface perturbations, PertAna
Model version	*3.2.1*	*4.1.1*	

2.5 IceLoss2.0

Kjeller Vindteknikk has developed the IceLoss2.0 model to calculate the power production losses due to icing. It uses data from The Numerical Weather Prediction model WRF as input, along with turbine specifics such as power curve, rpm curve, terrain elevation of each wind turbine, hub height and blade diameter.

2.5.1 Downscaling to Reduce Interval Variability.

The meteorological variables and topography within each grid are represented as a grid average. When using NWPs with spatial resolution 2.5-4 km, it fails to detect the local variabilities within each grid. The processes implemented in IceLoss2.0 to reduce this variability follows (Lindvall, 2017)

- Downscaling wind (speed and direction) to 1x1 km
- Cloud water adjustment due to orographic lifting (CWO)
- Cloud water sheltering (CWS)
- (Wake) reduced wind speed.

2.5.1.1 Downscaling Wind Speed and Direction

KVT has, in conjunction with creating wind maps covering Nordic countries, done several WRF simulations with a 1 km horizontal resolution. These simulations cover 1-2 years and have been long-term adjusted with a reference dataset. Now these simulations are used in IceLoss2.0 to downscale wind speed and direction from WRF 4x4 km to a 1 km resolution. For each turbine, the closest 1 km is located. Further, the wind direction and speed are downscaled by the U&N method (Liléo et al., 2013; Lindvall, 2017). This is a long-term correction method primarily based on a quantile regression technique. The downscaling of wind method described here with 1 km WRF simulations are only available for WRF data. That is, for IceLoss2.0 simulations with input data from the MEPS model, this downscaling feature is skipped.

2.5.1.2 Cloud Water Adjustment due to Orographic Lifting (CWO)

As the horizontal resolution for input data are 2.5 km (MEPS) and 4 km (WRF hindcast, WRF forecast), the terrain is smoothed with this resolution. For complex terrain, the difference between the real terrain height and this smoothed model height can be large. When air mass is forced upward due to rising terrain, the air mass is adiabatically cooled. If the air is humid, orographic clouds will form (Ahrens & Henson, 2020). As this is an important parameter for icing, the cloud water content needs to be adjusted due to this lifting. Firstly, temperature and air pressure are corrected to their actual height for each wind turbine, by picking out these variables at the correct height above sea level. The liquid water content, however, is lifted adiabatically from model height H to the wind turbines real height (H + h). Temperature typically decreases with height, causing the lifted air mass to condensate and form clouds. For a certain water content threshold, the excess water content is transmitted into precipitation. Figure 2-6 below depicts a schematic of cloud condensate lifting.
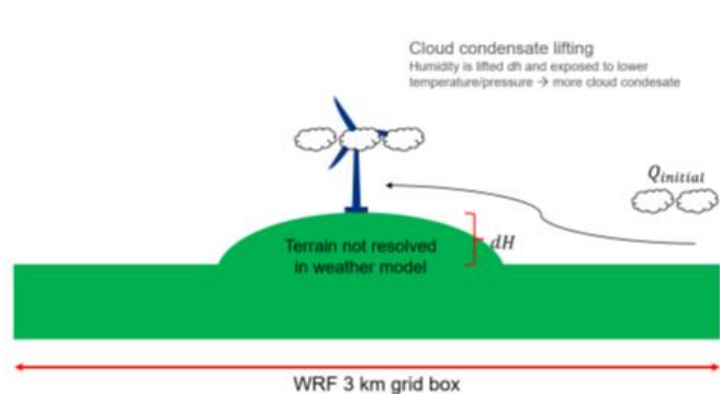
Figure 2-6 Illustration of orographic lifting method implemented in IceLoss2.0 (Lindvall, 2017).

2.5.1.3 Cloud Water Sheltering (CWS)

On the leeward side of a mountain the opposite effect of orographic lifting occurs, namely Foehn Warming. This is a result of accelerating downslope wind where the air mass is warmed and dried due to adiabatic descending. Foehn Warming is often recognized as warm weather and clear skies on the lee side of a mountain (Ahrens & Henson, 2020). As opposed to CWO, this effect gives a reduction of wind turbine icing. A schematic of how the cloud water content is adjusted due to Foehn warming is shown in Figure 2-7. Here, $Q_{initial}$ is the initial cloud water content adjusted by CWO, and Q_{new} is the cloud water content of the lee side. When passing the mountain or hill, the cloud water content is scaled by a reduction factor R.
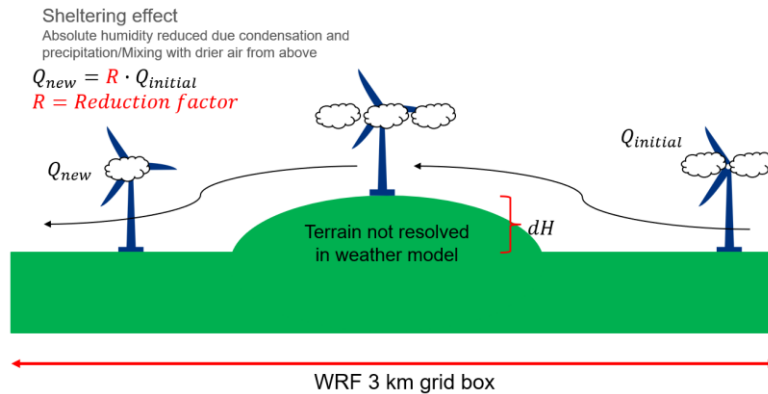
Figure 2-7 Illustration of how the Cloud Water Sheltering is calculated in IceLoss2.0 (Lindvall, 2017).

The reduction factor is defined as the ratio of $Q_{initial}$ to Q_{new}. This ratio was determined from a study using SCADA data from two wind farms along with high resolution WRF data (300m). At these sites, 40 transects across hills were defined and the relationship between Q initial and Q new were identified. The transects showed a clear relationship between the height of the hill.

The reduction factor is a scalar ratio that was obtained by investigating the cloud water content on each side of forty hills by following a direct transect over the hill as figure x illustrates. This revealed that the ratio was dependent on the height of the hill.

$$R = f(dH) \tag{1}$$
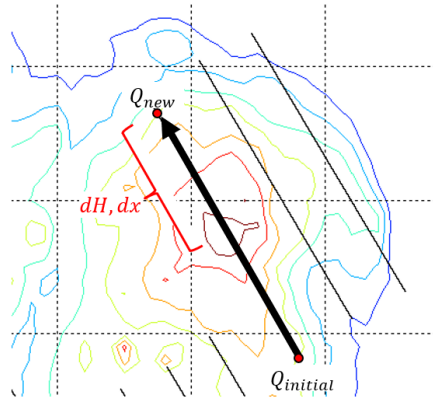
Figure 2-8 Example transect that was used to find the reduction factor R in IceLoss2.0. dH is the difference in elevation between Q $_{initial}$ and the top of the hill. dx is the horizontal distance between the top of the hill and Q$_{new}$. (Lindvall, 2017).

The height difference dH is obtained by topography maps with a 3 km diameter around each turbine. This is the difference between average elevation in each azimuthal direction and the elevation of the wind turbine.

2.5.1.4 (Wake) Reduced Wind Speed

If the nacelle wind speeds are provided by the WFs, the reduced wind speed by wake loss is accounted for in the IceLoss2.0 model. This is an optional feature only used if information about wake loss within the WF is available. If wake reduced wind speed is provided, it is accounted for by the U&N quantile regression method (Liléo et al., 2013). As previously mentioned, this method is used to downscale the wind speed and direction from a reference dataset to 1 km resolution. Now this method is used to downscale the wind speed a secondary time to the nacelle anemometer. (Lindvall, 2017). However, often only the "free mean wind speed" is provided from the WFs. Here the wake loss is not included, but this information is also used to downscale the wind speeds additionally.

2.5.2 Blade Cylinder Model

There are two ways the IceLoss2.0 model calculates the ice load. The first method is based on ISO12494 standard and was initially used for IceLoss1.0 (Lindvall, 2017). This method calculated the ice load on a standard cylinder that is 1 meter long, 3cm in diameter and is oriented vertically. Ice formation is due to particles in the air colliding with the cylinder. These particles can be either in liquid form, solid form, or a mixture of those two. Sources of ice that forms on structures include cloud droplets, rain drops, snow and water vapor

(ISO12494, 2017). The icing rate on a standard cylinder, according to ISO12494, is defined as

$$\frac{\mathrm{d}M_{std}}{\mathrm{d}t} = \alpha_1 \cdot \alpha_2 \cdot \alpha_3 \cdot w \cdot A \cdot V \tag{2}$$

where α_1 is the collision efficiency, α_2 is the sticking efficiency, α_3 the accretion efficiency, w the liquid water content, A is the collision area and V is the wind speed (Clausen, 2017).

The efficiency factors α_1, α_2, and α_3 vary between 0 and 1, hence they represent the different processes that reduce the icing rate. Factor α_1 represents the efficiency of a collision of the particles. Hence α_1 describes the ratio between the number of particles colliding with the cylinder and the total amount of particles on the windward side (Molinder, 2021). Factor α_2 represents the sticking efficiency. That is the number of particles sticking to the cylinder versus the total amount colliding with the cylinder. Lastly factor α_3 represents the accretion efficiency. This factor describes how much of the water or ice particle sticks to the cylinder. Example, if all the water droplets that collide with the cylinder sticks and freezes, the efficiency is one, if a part of the droplet runs off the surface before freezing, the efficiency is less than one. (ISO12494, 2017)

Although IceLoss2.0 also has an improved way of modelling the turbine blade ice load, it is primarily based on this theoretical modelling of icing on a standard cylinder. The improved methodology of calculating the ice load is called the blade cylinder model. This model consists of three cylinders oriented in such a way that the wind turbine blades are rotating in the same matter. Figure 2-9 shows a schematic of this model.
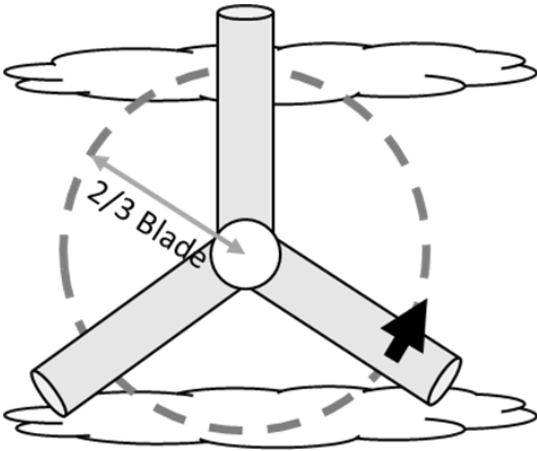

Figure 2-9 Schematic of the Kjeller Vindteknikk Blade Cylinder Model (Lindvall, 2017)

The icing rate equation for the blade cylinder model is then rewritten as

$$\frac{\mathrm{d}M_{blade}}{\mathrm{dt}} = \alpha_{1*} \cdot \alpha_2 \cdot \alpha_3 \cdot \mathrm{w} \cdot A_{blade} \cdot V_{air} \tag{3}$$

where V_{air} is the relative air speed, Ablade is the collision area of a cylinder representing the leading edge of a wind turbine blade. The collision efficiency α_{1*} is rewritten to better describe the collision process of an airfoil (Kjeller Vindteknikk, n.d.-a).

As the turbines rpm determines the relative wind speed in equation 3 the turbines rpm-curve is an important input parameter in the IceLoss2.0 model as well as other turbine specifics such as blade diameter. The liquid water content is also an important parameter in the IceLoss2.0 model as Equation 3 shows.

Ice is removed either by melting, sublimation, or shedding. These rates are determined by temperature, wind speed, radiation, relative humidity, and air pressure.

2.5.3 Energy Production Calculations

The full energy production numbers are calculated using the wind turbine specific power curve together with the modelled wind speed for each wind turbine. For production with ice or production with deicing, the full production is scaled by a reduction factor from 0 to 1. Where 1 is no reduction and 0 is standstill. This reduction matrix has been calibrated by a large database of historical icing losses from operational wind farms. This database consists of 24 wind farms located in Norway, Sweden, and Finland. The average period of assessment of historical icing losses from SCADA data is 4,6 years (Lindvall, 2017).

The reduction matrix is related to the variables wind speed, the accumulated ice mass on the blade cylinder and the icing intensity of the blade cylinder. It is calibrated by an iterative process where the icing losses from SCADA data and the IceLoss2.0 model are compared. This process is iterated until no improvement can be seen between the observed and modelled icing losses (Lindvall, 2017).

There are three parameters used to tune the reduction matrix. These are the ice mass ratio, icing intensity regimes and the revised cut in speed. The ice mass ratio defines the power reduction at different icing loads. The icing intensity regimes also determine the gravity of power production with active icing (Lindvall, 2017). The cut-in wind speed, that is the minimum wind speed for starting the wind turbine generator, is increased when icing occurs

as the weight of the ice would increase the blades inertia. Figure 2-10 illustrates how the wind speed, icing intensity and ice load affect the power curve. It shows three different 3D power curves with respect to wind speed and icing load. In addition, the magnitude of the power curve is reduced with increasing ice intensity, as the three different power curves demonstrate.
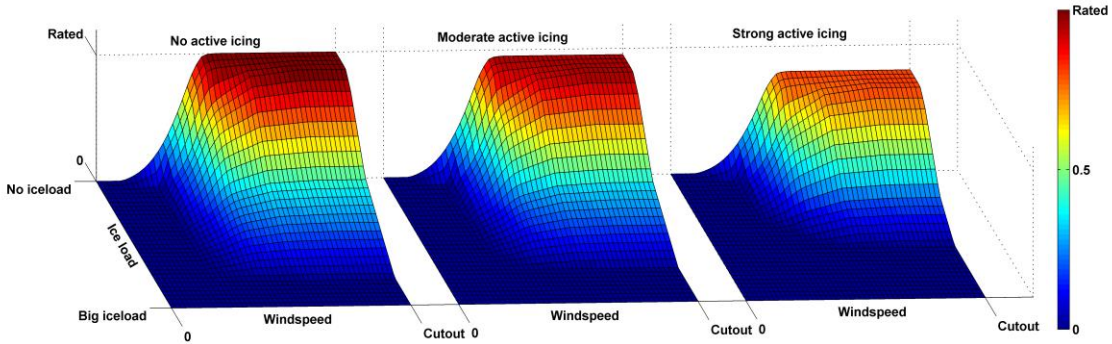
Figure 2-10: Illustration of the relationship between ice load, windspeed and icing intensity and their effect on the power curve. (Rissanen, 2023)

Note that the reduction matrix in IceLoss2.0 is tuned with icing losses from IceLoss2.0 where historical WRF simulations such as KVT Meso forecast have been used, as this is the NWP model that IceLoss2.0 is built upon.

Theres are several different reduction matrixes for the turbines with different types of deicing systems. The desired deicing system must be stated along with the other turbine data that goes into IceLoss2.0.

2.6 Analysis

2.6.1 Quantile-Quantile Plotting

The QQ plot or Quantile-Quantile plot is a graphical technique used to compare two distributions by plotting their quantiles up against each other. From '*Probability and Statistics for Engineers and Scientists'* (Warpole et al., 2014) the strict definition of a quantile is defined as follows "*A quantile of a sample, q(f), is a value for which the a specified fraction f of the data values is less than or equal to q(f)*". Essentially this means that quantiles are equally divided into groups of the whole distribution or dataset. If the two distributions plotted in a QQ plot are equal, the QQ plot would appear as a 45-degree line. Figure 2-11 show an example QQ plot of the temperature distribution from MEPS ensemble member 1 and from KVT Meso Hindcast. The red line if the 45-degree reference line while the blue dots

are the quantiles plotted. At low temperatures the quantiles are underneath the reference line, suggesting that the temperatures from MEPS data are higher than from KVT Meso hindcast. Above 266 K the quantiles are above the reference line, suggesting that KVT Meso has higher values (or in this case temperatures) than MEPS member 1. This way it is easy to detect differences between two datasets by comparing the datapoints to the reference line. As shown in the example, the QQ plotting method is used in this work to detect differences between the variables of the different input datasets that are used in IceLoss2.0.
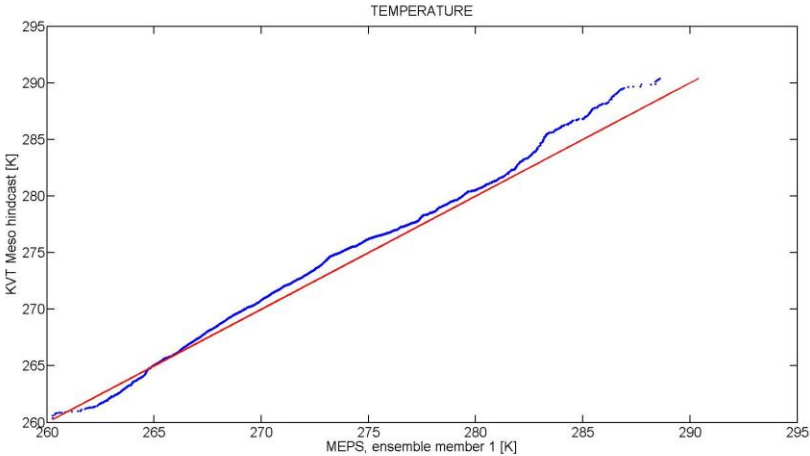
Figure 2-11: Quantile-Quantile plot of temperature quantiles from KVT Meso hindcast and MEPS ensemble member 1.

When comparing two datasets like the one in the example above, it is important to filter out data that might create biases. In this instance, the missing dates from MEPS ensemble member 1 also must be removed for the temperature dataset from KVT Meso hindcast. In other instances, zero- or NaN-values in dataset 1 are filtered out and so are the corresponding dates to these values removed from dataset 2. That way biases are avoided to best compare two 'clean' datasets.

2.6.2 Icing Loss and Energy Production

The relative icing losses are calculated as follows.

$$Icing\ Loss\ [\%] = \frac{Potential\ Energy\ Production - Partial\ Production\ with\ Ice}{Potential\ Energy\ Production} \cdot 100\% \quad (4)$$

Here 'Potential Energy Production' is the full potential power production without icing, 'Icing Loss' is the power production loss due to icing, and 'Partial Production' is the power production while icing may occur.

Iceloss2.0 has a temporal resolution of 1 hour. That means that the power produced at each timestep is the total energy produced within that hour. The production variables, that is, potential energy production, partial production with ice and partial production with ice and deicing, are the sum of all timesteps within the set timeframe. If days of data are missing, the production on these days is set to zero. Therefore, missing data alters the total energy production within the timeframe.

3 Method

3.1 Preparing Input Data

3.1.1 Extracting Variable

Both KVT Meso forecast, and MEPS data contain numerous variables, but not all are needed for icing calculations. The table below lists all variables extracted from KVT Meso Forecast and MEPS for the purpose of IceLoss2.0. Note that some of the variables that are not extracted from both models are not strictly needed, i.e., QGRAUP, QICE, QSNOW and RAINNC, but may influence the result.

IceLoss2.0 was initially made for historical WRF simulations like KVT Meso hindcast. As some of the variables were not available in the other datasets, KVT Meso forecast and MEPS, an input id was made. This id was used in the IceLoss2.0 code to avoid errors regarding missing data variables and for individual calculations. For example, WRF forecast did not have the variable air pressure available, so this was calculated using *ZNU*, *MU* and *MUB*. For MEPS however, air pressure var already calculated and available. Table 3 below shows the input id corresponding to the different input data types. Further, gives an overview of the input variables extracted and used in IceLoss2.0. Even though 30 ensemble member s are available from MEPS data, ensemble member 1, which is the deterministic forecast is used mostly as an example when comparing to the other numerical weather prediction models. The deterministic forecast is the forecast without any initial conditions changed slightly as for the other ensemble members (Jan, 2021).

Table 3: Identification number used in IceLoss2.0 to identify the different input types.

	Input_type
KVT Meso hindcast	No value
KVT Meso forecast	1
MEPS	2

Table 4: Variables extracted and used as input in IceLoss2.0.

Variables extracted for IceLoss2.0		
WRF forecast	MEPS	Explanation
U	U	U-component of wind (along x-axis) [m/s]
V	V	V-component of wind (along y-axis) m/s]
FF	FF	Wind speed [m/s] Calculated from U and V
DD	DD	Wind direction [degrees]. Calculated from U and V
TEMPERATURE	TEMPERATURE	Temperature model levels [K]
CLDFRA		Total cloud cover [%]
MU		Perturbation of mass column. Used to calculate air pressure
MUB		Base value of mass column. Used to calculate air pressure.
	PRESSURE	Air pressure
P_TOP	p0	Air pressure at top level [Pa]
PSFC	PSFC	Surface Pressure [Pa]
QCLOUD	QCLOUD	Cloud water mixing ratio
QGRAUP		Graupel mixing ratio
QICE		Ice mixing ratio
QRAIN	QRAIN	Cloud rain mixing ratio
QSNOW		Snow mixing ratio
QVAPOR	QVAPOR	Specific humidity [kg/kg]
RAINNC		Daily non-convective precipitation [mm]
SWDOWN	SWDOWN	Downward shortwave flux at ground surface
WRF_HGT	HGT	Height of grid point [m]
Z	Z + (HGT*9.81)	Geopotential height above sea level
ZNU		Sigma value of full levels. Used to calculate air pressure.
ZNW		Sigma value of half levels.
jdate	jdate	Time variable. [Julian Date]
input_type	input_type	Used for IceLoss2.0 to recognize the different input data types.

As mentioned above, some variables needed to be calculated from the existing variables in above. These variables are wind speed *FF*, wind direction *DD* and additionally for KVT Meso forecast, air pressure *p*. The equations used to obtain these variables are listed below.

$$FF = \sqrt{U^2 + V^2} \tag{5}$$

$$DD = 270 - \arctan(V, U) \cdot \frac{180}{\pi} \tag{6}$$

$$muT = MU + MUB \tag{7}$$

$$p = ZNU \cdot muT + P\_TOP \tag{8}$$

Where *muT* is the total mass in each column and *p* is the calculated air pressure for KVT Meso simulations. The remaining variables are explained in Table 4 above.

When investigating the variables from MEPS, it became clear that the order of elevation levels where on the opposite order than KVT Meso data. For example, the variable '*PRESSURE*' increased with height level, which clearly does not correlate with reality. Since IceLoss2.0 was originally made for KVT Meso hindcast, the model interprets the data with an increasing height for each model level. All variables from MEPS data with a height dimension, had to be flipped to represent the right order of height levels.

3.1.2 Creating Winter Timeseries

When running IceLoss2.0 for one forecast, the ice load on the turbine blades is initially set to 0 grams. Ideally this should have been corrected to current ice load with SCADA data for every Iceloss2.0 forecast simulation. Another solution to avoid all forecasts starting with ice load at 0 grams, is to combine all forecasts into one coherent time series and use this as the IceLoss2.0 data input. However, the limitation here is that ice load offsets accumulate over icing episodes as they are not adjusted with SCADA data. Even so, this solution is better than resetting the ice load for each forecast, as it would lead to an underestimate of icing loss. This is a simplistic approach for this work to test if the data could be used to make icing forecast at all. The timeframe for the winter timeseries was chosen to be from 14th September 2021 to 1st of June 2022, which is a total of 262 days or 6288 hours.

MEPS forecast data has a lead time of 62 hours, that is, the forecast applies to the following 62 hours from its starting time. New forecasts are generated every six hours, at 00:00, 06:00, 12:00, and 18:00 each day. Energy producers must deliver their day ahead production estimate at 12:00, so the earliest forecast available is from 06:00 (lead time 18 to 42). Some days all four MEPS forecasts are missing, and the earliest possible forecast is then from 18:00 the day before (lead time 30 to 54). Lastly, there are some days that MEPS data is missing altogether, and forecasts cannot be made. This accounts for 11% of the timeseries. These dates are listed in Table 6 below. Note that almost half of the missing dates are in January, a knowingly cold month. Having so many dates missing in the winter year could affect the icing losses in a positive way.

Table 5: List of missing dates from the MEPS data winter timeseries.

	Missing dates from MEPS data
1	14.09.21
2	15.09.21
3	04.11.21
4	05.11.21
5	30.11.21
6	09.12.21
7	19.12.21
8	20.12.21
9	05.01.22
10	07.01.22
11	08.01.22
12	09.01.22
13	16.01.22
14	17.01.22
15	18.01.22
16	25.01.22
17	26.01.22
18	27.01.22
19	28.01.22
20	29.01.22
21	30.01.22
22	31.01.22
23	03.02.22
24	06.02.22
25	07.02.22
26	12.02.22
27	06.03.22
28	07.03.22
29	27.05.22

In addition, most members had some dates where data was available, but it contained NaN-values. These dates also needed to be removed from the winter timeseries, as IceLoss2.0 does not accept NaN-values. These extra missing dates are listed in REF in the Appendix section.

KVT Meso forecast data has a lead time of 49 hours. As with MEPS data the earliest available forecast is the 06-forecast the day before the forecast date. But when data is missing, the only chance to retrieve it is by looking at the previous forecast 6 hours before, that is at

time 00:00, with lead time 25 to 48. Luckily, not much data is missing from the WRF forecast. In this case only 5 out of 262 days were missing. This accounts for 1.2% of the days.

Table 6: List of missing dates from the KVT Meso forecast data winter timeseries.

Missing dates KVT Meso forecast	
1	31.10.2021
2	12.12.2021
3	13.12.2021
4	30.12.2021
5	31.12.2021

3.2 Model Setup

In this work only the icing loss of one turbine at Kvitfjell and Raudfjell WFs are investigated, namely turbine KN04. This turbine was chosen because it was one of the turbines investigated in the IceLoss2.0 validation project paper by the author. That means that IceLoss2.0 simulations with KVT Meso hindcast setup was already available and could be used as a baseline. KN04 was only one of eight turbines used in the validations, but it is investigated further in this work due to its elevation. It is located at 523.2 mas and should therefore be one of the turbines at Kvitfjell Wind Farm that is most exposed to icing.

Table 7: Turbine specifics for IceLoss2.0.

WTG	Longitude	Latitude	Elevation	WT type	Hub height
KN04	621645	7723109	523,2	SWT-DD-130-4,2	85

Some other turbines were added into the input file as well, due to some unknown error codes from IceLoss2.0 when only running for one turbine. These are not listed here as they are not relevant for this work and will not be investigated further.

The turbine specific power curve was also added. A plot of this is shown in Figure 3-1 below.
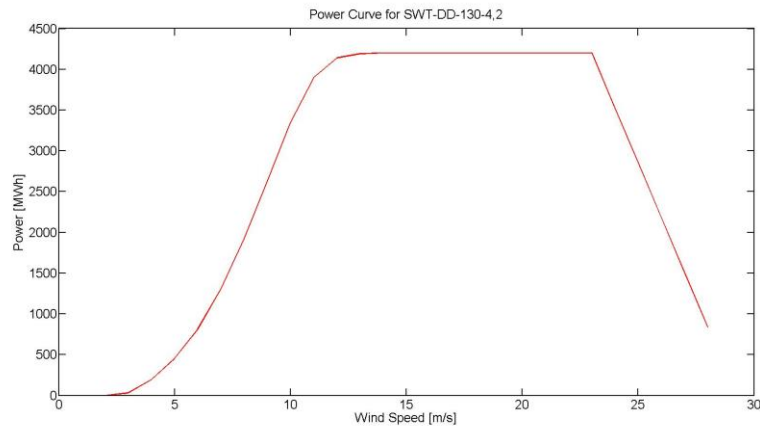
Figure 3-1: Manufacturer power curve for turbines SWT-DD-130-4,2

The deicing system in IceLoss2.0 was set to 'N149'. This actually corresponds to turbines produced by Nordex, but has proven to be a better fit for these specific turbines (Byrkjedal, 2022)

3.3 Scaling Input Variables

A good exercise when investigating the different input variables from the three NWP models and their impact on the ice calculating, is changing the variables slightly and seeing how this changes the icing losses.

Since three different NWP models are used as input for IceLoss2.0, their variables are compared to each other in the QQ plots. If model 1 provides better icing loss results than model 2 and 3, one can scale some of the variables from these two models to correlate better with the variables from model 1. By scaling one variable at a time and investigating the change in icing loss, it is easier to determine the variables influence on the icing losses.

The QQ plots are used as a starting point when finding a good scaling factor for the variables. Figure 3-2 visualizes this scaling of an example variable x with respect to the QQ plot reference line. Here the blue dots are the original QQ plot, while the green dots represent the new QQ plot where Variable x from Model 1 are scaled by 1.3. This way, Variable x from Model 1 is scaled to the same magnitude as Variable x from Model 2. The two variable distributions are now more alike. If the icing losses also are closer to each other by this scaling, it is apparent that the difference in variable x from the two models were the cause of the differences in icing loss.
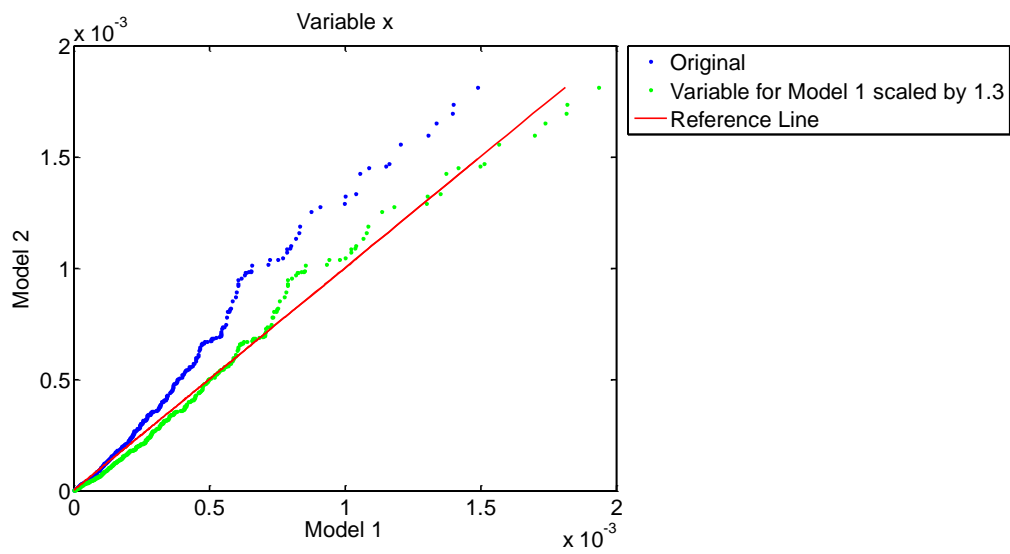
Figure 3-2 Example QQ plot of variable x from NWP model 1 and 2. The blue dots refer to the original QQ plot. The green dots are the new QQ plot where variable x from Model 1 is scaled by a factor of 1.3. This scaling factor is used as an analytic tool when investigating the impact of icing from each variable.

4 Results and Discussions

4.1 Icing Losses

Table 8 below represents the icing losses from IceLoss2.0 using the three different input datasets, KVT Meso hindcast, KVT Meso forecast and MEPS. These results show an icing loss of 3,34% for KVT Meso hindcast, 3,42% for KVT Meso forecast and 1,80% for MEPS ensemble member 1. However, the timeframe for the calculation of these losses is not the same due to the missing dates in KVT Meso forecast and MEPS. When filtering out these missing dates from all production time series, KVT Meso hindcast has an icing loss of 3,18% without deicing, KVT Meso forecast 2,98% and MEPS 1,83%. Proving that when the size of time series are equal for all datasets, KVT Meso hindcast still has the highest losses while MEPS ensemble member 1 has the lowest losses. This trend is also true for icing losses with an active deicing system shown in Table 8.

Table 8: Icing losses from IceLoss2.0 with three different input datasets, KVT Meso hindcast, KVT Meso forecast and MEPS ensemble member 1.

Input data	Icing loss	Icing loss w/deicing
KVT Meso hindcast	3,34%	2,58%
KVT Meso forecast	3,42%	2,61%
MEPS member 1	1,80%	1,23%

The icing losses with KVT Meso hindcast are considered the most trustworthy, both due to its statistical advantage, and due to the fact the IceLoss2.0 was written and corrected with respect to this type of dataset. However, in an IceLoss2.0 validation where this specific turbine was investigated, the SCADA data suggested an icing loss of 2,3 % with deicing, while the IceLoss2.0 model with KVT Meso hindcast suggested an icing loss of 3.3% with deicing (Andersen, 2022). Here the KVT Meso hindcast model overestimated the icing losses. The timeframe for this validation was from mid-February 2021 to mid-February 2022. Note that because this timeframe is extending over a full year, the icing losses could therefore be lower since summer months are included. Also note that half of the timeframe is within the same timeframe investigated in this work. With these results in mind, both KVT Meso hindcast and KVT Meso forecast seem to be closer to reality than MEPS. However, this should be confirmed by looking at SCADA data from the same period that is simulated here. Considering both KVT Meso hindcast and KVT Meso forecast are WRF simulations, it is not surprising that these provide similar icing losses.

For all these simulations, the icing losses are higher without deicing as Table 8 shows. This implies that all simulations contain episodes with sufficient icing to make the deicing module efficient. Meaning that all IceLoss2.0 simulations with different input datasets have had success with ice buildup. This is good confirmation that the model works for all these different types of input data. Now the question lies within the accuracy of these results.

Simulations with MEPS data as input have the lowest icing losses. Due to the experience with KVT Meso hindcast, this loss is considered too low. It is important to bear in mind that the power reduction matrix used to calculate the icing loss from the ice load is tuned with KVT Meso hindcast input data. This reduction matrix needs to be adjusted for MEPS data as well.

The following Table 9 shows the energy production numbers, potentially, with icing, and with ice and an active deicing system. These numbers are the sum of energy production within the investigated timeframe, 14th of September 2021 to 2nd of June 2022. The production numbers are of the same magnitude for all input types, although their differences vary up to 2601 MW.

Table 9: Energy Production numbers for three different IceLoss2.0 simulations using three different input datasets, KVT Meso hindcast, KVT Meso forecast, and MEPS ensemble member 1.

Model	Potential production [MW]	Production with icing [MW]	Production with ice and deicing [MW]
KVT Meso hindcast	12118	11713	11806
KVT Meso forecast	14719	14216	14335
MEPS member 1	13350	13110	13186

As the energy production numbers in Table 9 are only the sum of production during the set timeframe, it is important to recall that MEPS ensemble member 1 are missing 11.5% of the dates for the total dataset. Therefore, the energy production numbers for MEPS member 1 should have been higher. The same goes for KVT Meso forecast, but this dataset is only missing 1,2% days of data which is hardly noticeable.

Table 10: Icing loss statistics from all 30 ensemble member in the MEPS input dataset.

	Icing loss distribution [%]	Icing loss with deicing distribution [%]
Mean	1,77	1,47
Median	1,80	1,48
Minimum loss	1,41	1,23
Maximum loss	2,32	1,74
Range	0,91	0.51
Standard deviation	0,21	0.14

Continuing investigating the MEPS ensemble data. Table 10 above present some statistics of icing losses from the whole set of ensembles. By looking at the minimum and maximum icing loss, it becomes evident that the icing loss differs with less than 1%. The standard deviation for the icing loss distribution is 0,21%. Further, the median and mean loss are close, that is they only differ up to 0,03%. This again proves that there are no extreme values in this dataset shifting the central calculations, as Figure 4-1 shows. The figure also shows that member 6 provides the minimum icing loss, member 26 has the maximum icing loss. The icing loss from member 1 shown in Table 8 are also the median icing loss. These three members will be used in icing loss timeseries Figure 4-9 to see the difference between the maxima, minima, and median ensemble.
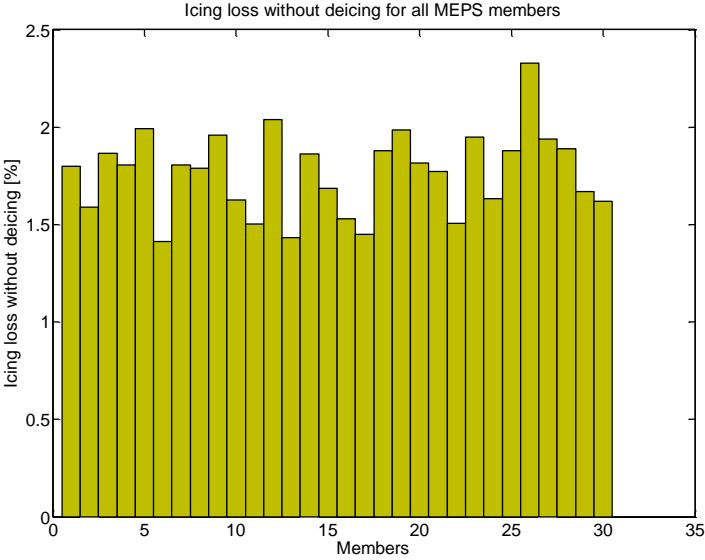

Figure 4-1: Distribution of icing loss without deicing [%] for all 30 MEPS ensemble members.

4.2 Comparisons of Input Variables

One way to identify what is causing these differences in production and icing loss, is by comparing the input variables to each other. KVT Meso forecast and MEPS ensemble 1 are compared to KVT Meso hindcast as this is the dataset originally used by IceLoss2.0. Temperature and wind speed are compared at approximately hub height which is 608 mas. For KVT Meso simulations that is at model level 3, which corresponds to 586 mas for KVT Meso hindcast and 559 mas for KVT Meso forecast. For MEPS simulations level 9 corresponds to 590 mas. Mixing ratios that are used to determine liquid water content is compared at model height. This is because the variables that are extracted undergo orographic lifting and cloud water sheltering as mentioned in the theory section. Table 11 below

summarizes the level height used in the variable comparisons. The following sections go through some of the variables that have greatest impact on icing.

Table 11: Extracted model levels and their corresponding height above sea level. Variables used for comparison are extracted at these levels.

Model	Level number	Level height + model height [mas]
KVT Meso hindcast	3	586
KVT Meso forecast	3	559
MEPS member 1	9	590
KVT Meso hindcast	1	253
KVT Meso forecast	1	224
MEPS member 1	1	362

4.2.1 Temperature

Temperature is one of the most important variables when investigating icing. For example, temperature determines if cloud droplets are subcooled and freeze on the blades or not. Temperature also affects melting, sublimation, and shedding. Figure 4-2 below shows the QQ plot of Temperatures from KVT Meso forecast and MEPS up against temperatures from KVT Meso hindcast. This shows that both distributions are fairly but not perfectly close to the reference line.

(a)   *(b)*
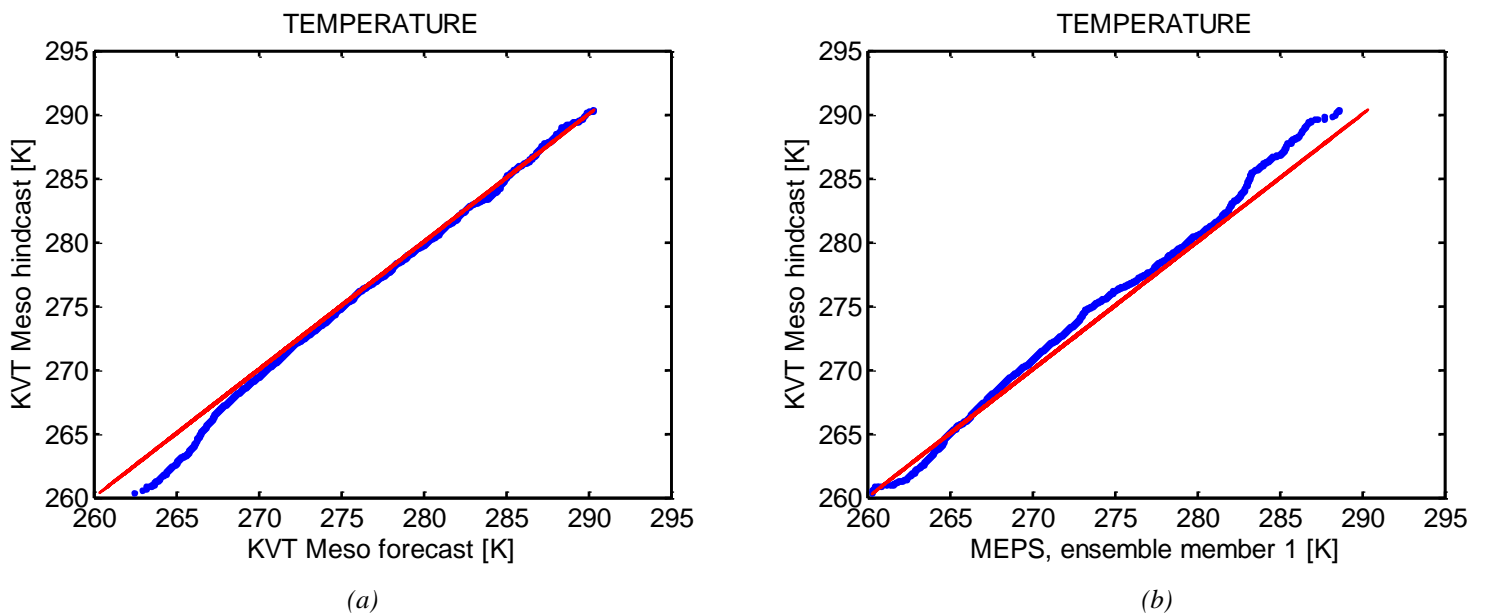
Figure 4-2: QQ plots of temperatures at approximately hub height. Figure (a) is the QQ plot of temperatures from KVT Meso hindcast and KVT Meso forecast. Figure (b) is the QQ plot of temperatures from KVT Meso hindcast and MEPS. Temperature is extracted from approximately hub height.

Figure 4-1 (a) illustrates the comparison between KVT Meso hindcast and KVT Meso forecast. This shows that at temperatures below the freezing point 273 K (0ºC), KVT Meso

forecast has higher temperatures than KVT Meso hindcast. Above 273K the distributions seem to be similar.

Figure 4-2 (b) show the QQ plot between MEPS and KVT Meso hindcast temperatures. For most temperatures, the KVT Meso hindcast distribution has higher temperatures than MEPS, suggesting that the icing loss for MEPS should be higher than for KVT Meso hindcast. However, for temperatures between 261-265K (-12ºC to -8ºC) MEPS temperatures are higher than KVT Meso hindcast. Since this is way below the freezing point, is it reasonable to think that this does not affect the difference in icing. As the temperature QQ plot between KVT Meso hindcast and MEPS did not give an apparent reason for the difference in icing loss, the answer may lie in the other ice related variables.

4.2.2 Wind Speed (FF)

As shown in the icing rate equations (Equation 2 and 3), the wind speed has a direct effect on ice buildup. Wind speed affects the turbines rotational speed which in turn affects the number of collisions between the blades and the surrounding particles. An increase in wind speed would increase the number of collisions between blade and particle but also decreases the sticking efficiency. These contradictory effects on icing together with its dependence on other variables make it difficult to determine its positive or negative effect on icing. As an example, higher wind speeds would not lead to more icing if the temperature were above freezing point.

However, potential production is directly dependent on the wind speed. Investigating the differences in wind speed are therefore useful to confirm the differences in potential production from Table 9. When comparing the wind speeds in QQ plots, the main area of interest is between about 3m/s and 14 m/s. This refers to the slope of the turbine power curve in Figure 3-1: Manufacturer power curve for turbines SWT-DD-130-4,2. At wind speeds above 14 m/s the turbines produce at maximum and wind speed differences within this interval do not matter as the energy produced would remain the same. Above 23 m/s the energy production declines with wind speed, and again the wind speed differences cause differences in potential production.

Figure 4-3 below shows two QQ plots of wind speeds from KVT Meso hindcast in comparison with KVT Meso forecast (a) and MEPS (b). The wind speeds for KVT Meso hindcast and KVT Meso forecast are close to the reference line, meaning these distributions are similar up to 13 m/s. At that point the wind speeds from KVT Meso forecast seems to be

slightly higher than KVT Meso hindcast. At 25 m/s the distribution takes a sharp turn increasing the difference between the two distributions. Even though these wind speed distributions are close, their slight difference led to an energy production difference of 2601 MW (from Table 9). Proving that the IceLoss2.0 energy production calculations are highly sensitive to wind speed differences.
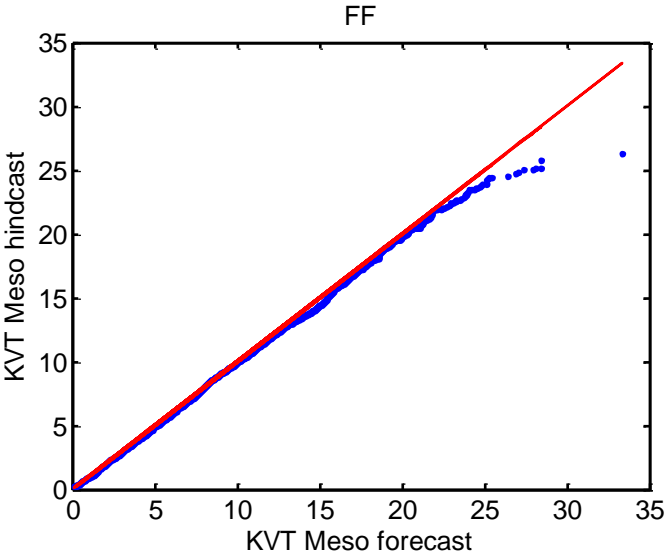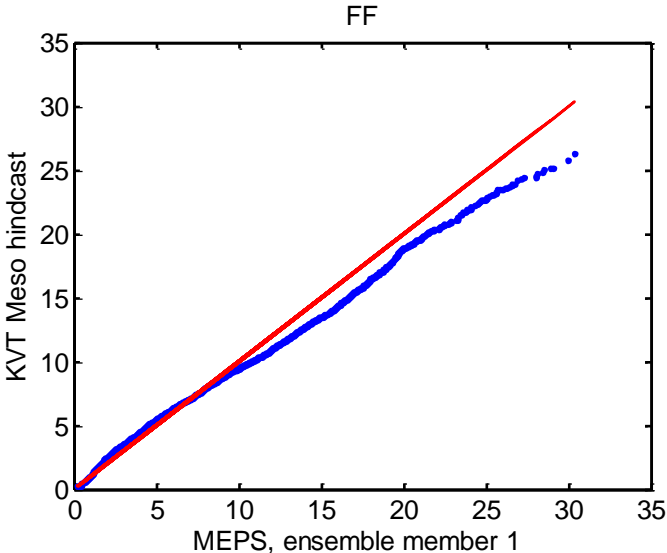

<div align="center">Figure 4-2 (a)   Figure 4-2 (b)</div>

Figure 4-3: QQ plots of Wind Speed FF [m/s] between KVT Meso hindcast and (a) KVT Meso forecast, and (b) MEPS. Wind speeds at extracted from approximately hub height. QQ plot distributions are marked as blue dots while the reference line is marked in red. Wind Speed FF is extracted from approximately hub height.

Figure 4-3 (b) display the QQ plot of Wind Speed FF from KVT Meso hindcast and MEPS. This plot shows that the wind speed from MEPS is higher than KVT Meso hindcast from 7 m/s and upwards, and this difference is increasing with wind speed. Below 7 m/s there is a slight shift towards KVT Meso hindcast, meaning the wind speed are slightly higher here. In short, the wind speed is mainly higher for MEPS than KVT Meso hindcast. This explains why the potential production in Table 9 is higher for MEPS.

Considering the wind speeds are highest from MEPS, this input model should give the highest potential energy production. However, recall that MEPS data has at least 11% of days missing from the winter timeseries. As the potential production is merely the sum of energy produced within the time series, the potential energy production from MEPS is missing a significant amount of energy produced.

4.2.3 Cloud Water Mixing Ratio (QCLOUD)

The variable QCLOUD is as states the cloud water mixing ratio. In other words, the fraction of cloud condensed water in the air. This is important for IceLoss2.0 to calculate the in-cloud icing. Figure 4-4 show the QQ plots of the cloud mixing ratio for KVT Meso hindcast compared to KVT Meso forecast and MEPS, respectively. Recall that zero and NaN-values were filtered out from these distributions before plotting the quantile. Here KVT Meso hindcast had 5843 out of 6288 timesteps with zero values and KVT Meso forecast had 5894 zero- and NaN-values. Lastly MEPS member 1 had only 2515 zero- and NaN-values. Already from the number of zero values, it becomes apparent that MEPS member 1 has higher cloud mixing ratio than KVT Meso hindcast, which Figure 4-4(b) also confirms for the remaining nonzero values as well. KVT Meso forecast also has a higher cloud mixing ratio than KVT Meso hindcast. It is believed that a higher cloud mixing ratio leads to more in-cloud icing if temperatures are low enough. This appears not to be the case here since KVT Meso hindcast has the lowest cloud mixing ratio but higher losses than MEPS (Table 8). But solely investigating the cloud mixing ratio does not give the whole picture of icing conditions, therefore more investigations are needed.
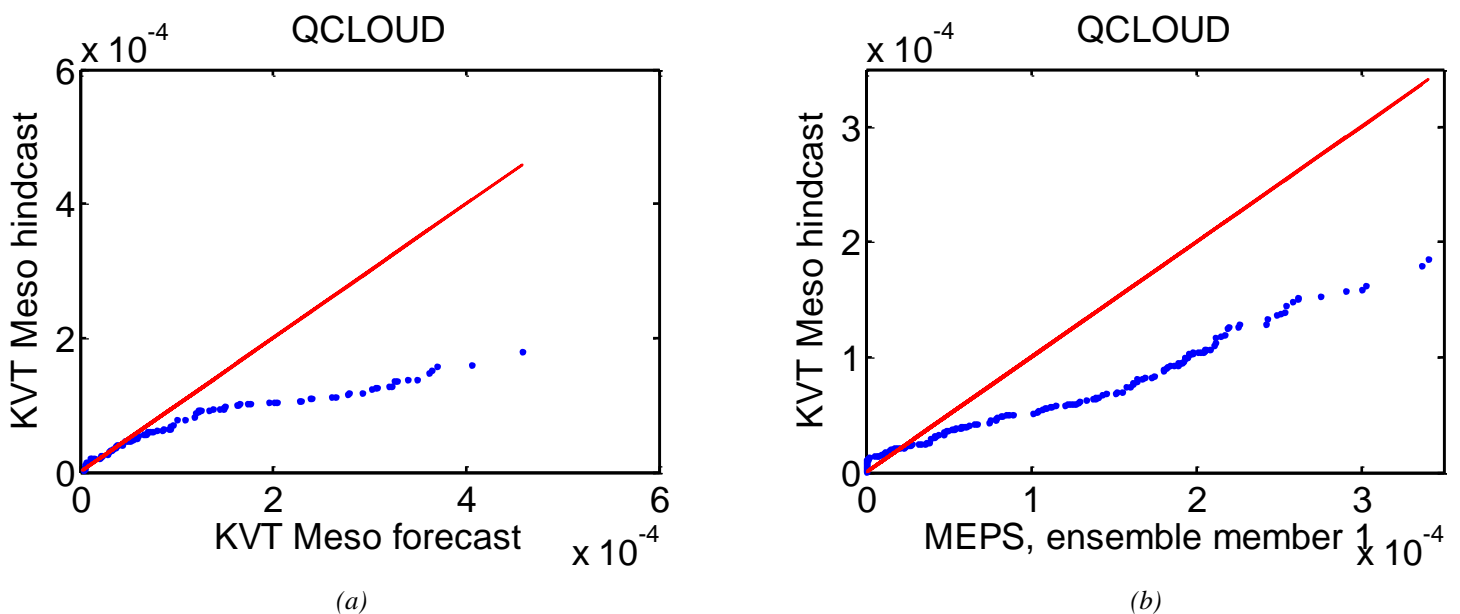

Figure 4-4: QQ plot of variable QCLOUD from KVT Meso hindcast and (a) KVT Meso forecast, and (b) MEPS member 1. The quantiles are plotted as blue dots while the reference line is red. QCLOUD is extracted from approximately model level.

4.2.4 Cloud Rain Mixing Ratio (QRAIN)

Cloud rain mixing ratio is another variable used to determine the liquid water content in Equations 2 and 3. Investigating the differences in this variable could also provide some insight into the icing loss differences between the different input models. Figure 4-5 depicts the relationship between KVT Meso hindcast and (a) KVT Meso forecast, and (b) MEPS ensemble member 1, for the variable rain mixing ratio (QRAIN). As the figure shows, there are few datapoints for this distribution. KVT Meso hindcast contain 5427 zero values of 6288 data points in total. Similarly, KVT Meso forecast contains 5475 zero values and MEPS contains 4106 zero values. Since this variable is zero over 65% of the time, its significance can be discussed. However, for the nonzero variables, the differences are shown as QQ plots in Figure 4-5. The difference between KVT Meso hindcast and KVT Meso forecast are low as Figure 4-5(a) shows, especially since they both have a similar amount of zero values as well. It is evident that the rain mixing ratio does not cause the differences in icing loss between these two input models.
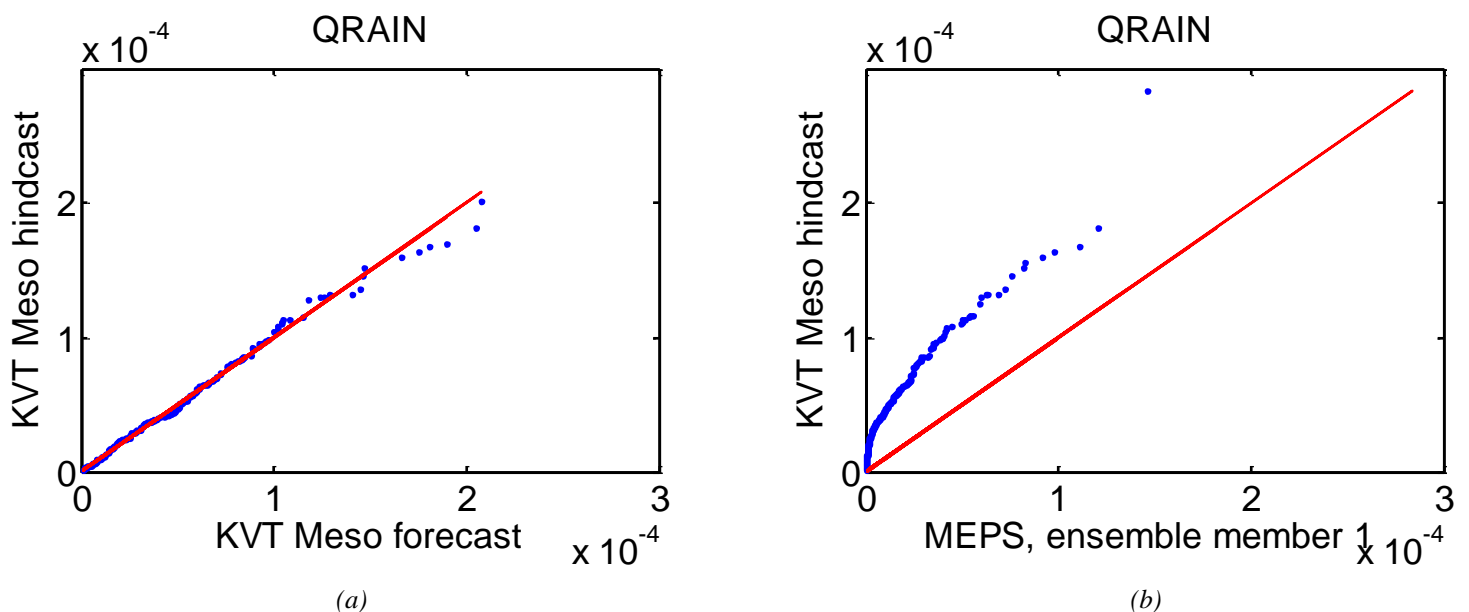
Figure 4-5: QQ plots of variable QRAIN, rain mixing ratio, comparing KVT Meso hindcast distribution to (a) KVT Meso forecast and (b) MEPS member 1. The variable is extracted at approximately model height. QQ plot distribution is marked with blue dots, and reference line in red.

For MEPS however, the rain mixing ratio is lower than KVT Meso hindcast as Figure 4-5(b) shows. To investigate its effect on icing, the scaling methodology previously described was tested. Figure 4-6 shows the original and scaled distribution. As MEPS is only scaled by one number it is difficult to make all quantiles fit the reference line, but as the figure shows a

scaling factor is 1.8 was chosen. The scaling factor only gave an increase in icing loss without deicing of 0,02%. It goes to show that this variable has some effect of the icing loss but is not the main cause of the low losses for the MEPS input model.

Figure 4-6: QQ plot of rain mixing ratio between KVT Meso hindcast and MEPS member 1. The original distributions are shown as blue dots, while the distributions where MEPS member one is scaled by 1.8 are shown in green dots. The red line is the reference line.

4.2.5 Specific Humidity (QVAPOR)

The last variable that influences the liquid water content w from Equations 2 and 3 is the specific humidity (QVAPOR). Figure 4-7 shows the differences in specific humidity between KVT Meso hindcast and (a) KVT Meso forecast, and (b) MEPS member 1.

QVAPOR

KVT Meso hindcast (y-axis) vs KVT Meso forecast (x-axis, x 10⁻³)

(a)

QVAPOR

KVT Meso hindcast (y-axis) vs MEPS, ensemble member 1 (x-axis, x 10⁻³)

(b)

Figure 4-7 : QQ plots of variable QVAPOR, specific humidity, comparing KVT Meso hindcast distribution to (a) KVT Meso forecast and (b) MEPS member 1. The variable is extracted at approximately model height. QQ plot distribution is marked with blue dots, and reference line in red.

The specific humidity for KVT Meso hindcast and KVT Meso forecast follows the reference line closely with some larger deviations up until $2 \cdot 10^{-3}$ where the specific humidity is larger for KVT Meso forecast. All in all, these distributions seem to be reasonably close.

Between KVT Meso hindcast and MEPS member 1 in Figure 4-7 (b) the QQ plot is more distinctively shifted towards the upper left corner. That is, the KVT Meso hindcast specific humidity seems to systematically be a little bit higher than for MEPS member 1. If the MEPS member 1 specific humidity is scaled by 1.1 as Figure 4-8 shows, the distributions align to the reference line. A scaling by 1.1 of the specific humidity for MEPS member 1, would lead to an icing loss of 11.53%. It is obvious that the specific humidity has a vast impact of the icing losses, when such a small scaling factor increases the icing loss by 9.7%.
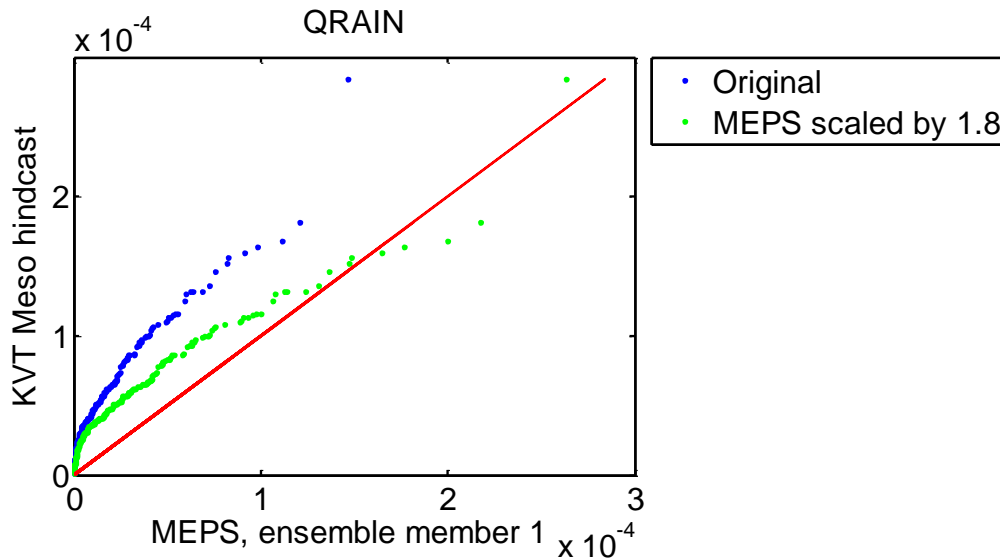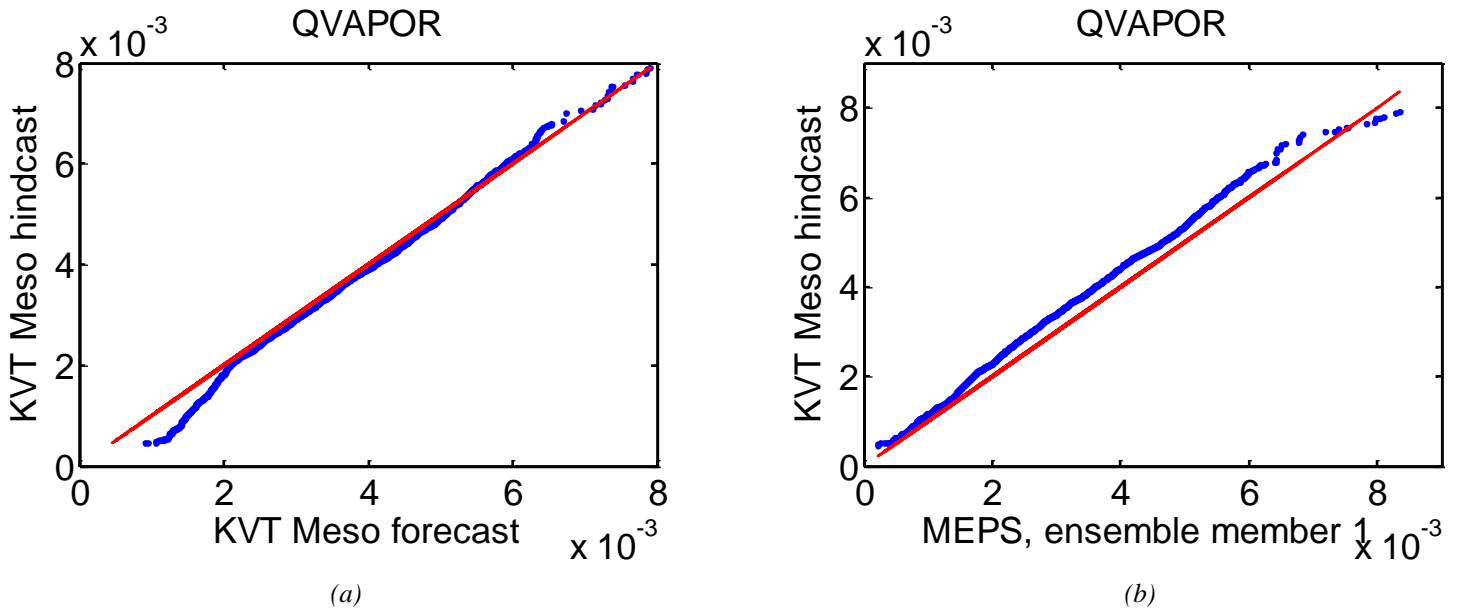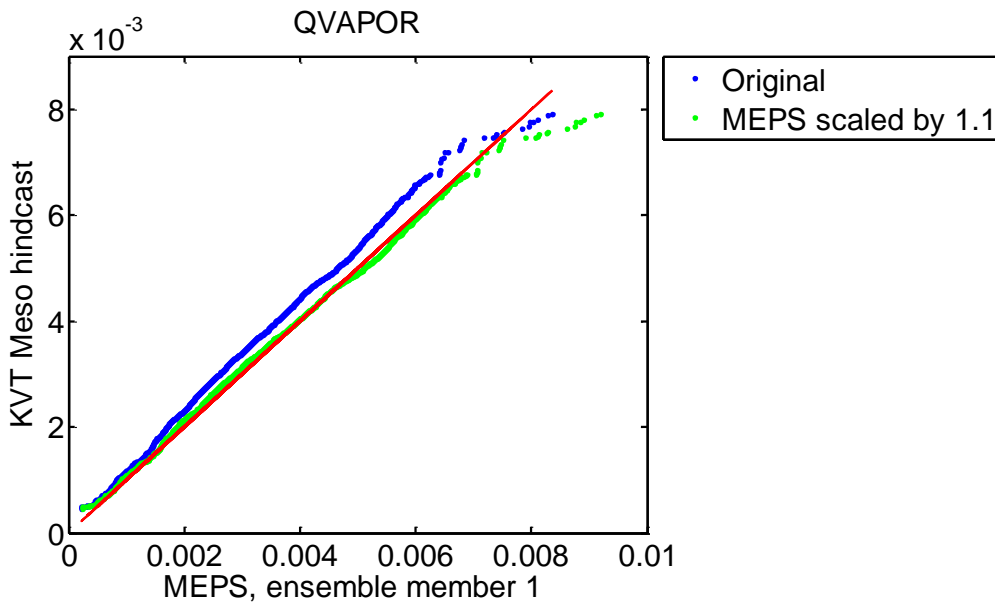
Figure 4-8: QQ plot of specific humidity between KVT Meso hindcast and MEPS member 1. The original distribution is shown as blue dots, while the distribution where MEPS member one is scaled by 1.1 are shown in green dots. The red line is the reference line.

The sensitivity of this variable shows that the scaling method might not be the best to tweak the results from IceLoss2.0 with MEPS as input. However, it does reveal the sensitivity of the input data and makes it easier to detect faults in the input data. If all variables investigated above, Temperature, FF, QCLOUD, QRAIN and QVAPOR were scaled with respect to KVT Meso hindcast, the resulting icing loss is expected to be the same as for KVT Meso hindcast, which might not even be the correct icing loss. The scaling methods could however be used to scale the icing loss according to SCADA data in the future to tweak its results.

4.3 Timeseries

4.3.1 Icing Losses

So far, the magnitude of the icing loss has been the main focus in this work, but another important aspect is the timing of the icing events. Figure 4-9 below shows 3 timeseries of the icing losses from KVT Meso hindcast, KVT Meso forecast and three MEPS members. The control member 1, member 6 which produced the total minimum icing loss, and ensemble member 26 which produced the total maximum icing loss from Table 10. The top one is a demonstration of the icing loss throughout the whole timeframe, while the others are more closely samples of some icing episodes. The different icing loss time series are shown in different colors are the figure legend shows, while the dates where MEPS data is missing is
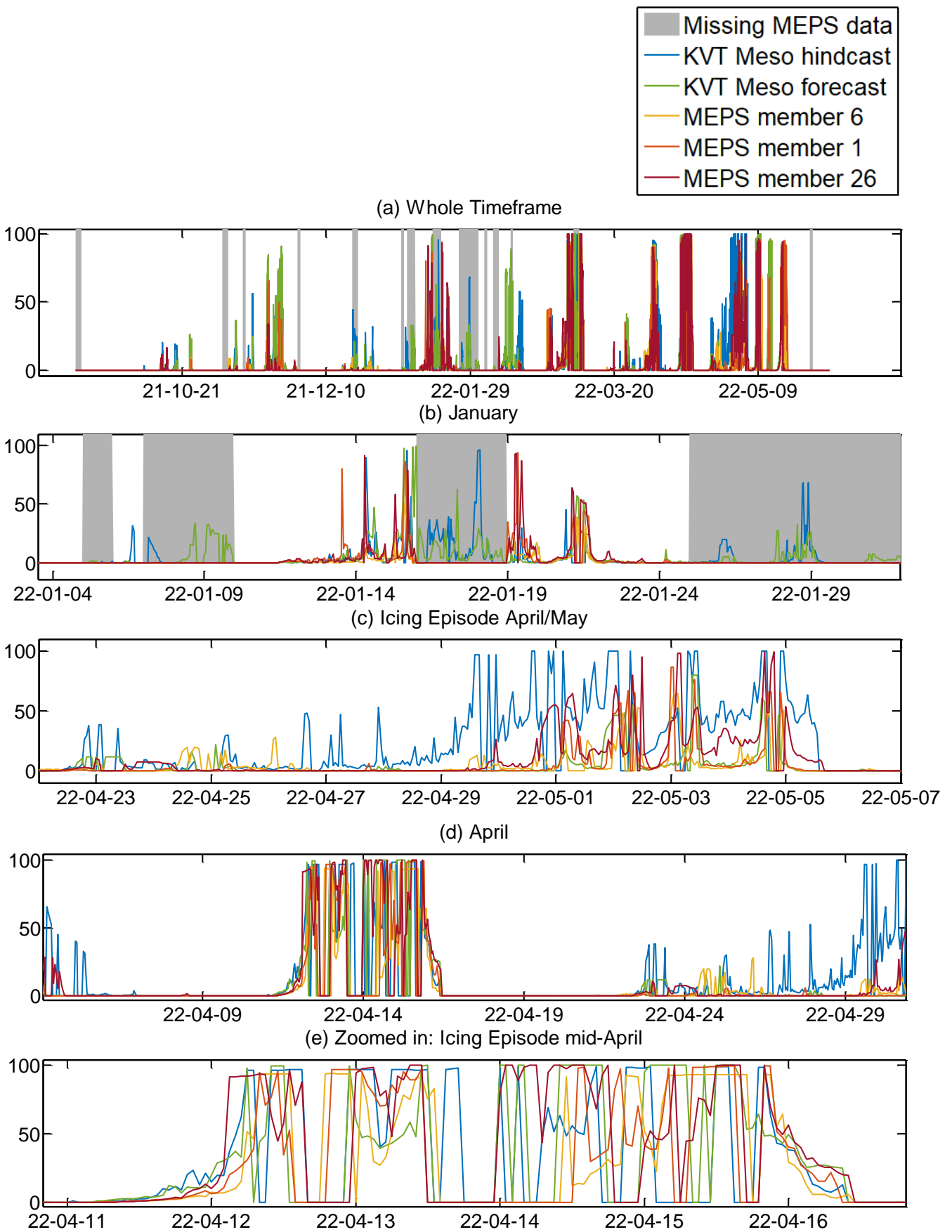
marked with a grey background.

Figure 4-9: Timeseries of icing losses from KVT Meso hindcast, KVT Meso forecast, and MEPS members 1, 6 and 26.

Figure 4-9 (a) shows that the icing loss throughout the whole timeframe. It shows that the first icing episode, or episode of significant icing to create an icing loss was in mid-October, while the last one being around mid-May. Both at the beginning and end of the timeseries there are no icing losses, suggesting that the timeseries has captured the whole winter and all its icing episodes.

Figure 4-9 (b) show several episodes in the beginning and end of January where both KVT Meso hindcast and KVT Meso forecast has provided an icing loss, while the MEPS member 1 data hardly provided any. As the grey background confirms, this month had a lot of missing MEPS data which lead to zero loss in the time series. This shows that the MEPS input data had several days of possible icing missing that could have increased the icing loss from Table 8.

A more severe icing episode from 23rd of April to 6th of May is shown Figure 4-9 (c), here the KVT Meso hindcast icing loss are significantly higher than KVT Meso forecast and MEPS. The three MEPS ensemble members depicted here also have a wider range, especially around 3rd of May to 6th of May. Icing episodes like these definitely contribute to the higher total icing loss for KVT Meso hindcast. For the spikes of high icing loss for KVT Meso forecast and MEPS, the timing seems to fit with some of the spikes from KVT Meso hindcast, although KVT Meso hindcast has more spikes than the other forecasts. However, with so many spikes within a short period of time it is difficult to determine if there is a time displacement between the five simulations depicted in this figure.

It is interesting to notice that within these episodes of heavy icing in Figure 4-9 (c), the icing loss oscillates rapidly between 100% and 0%. Note that the icing loss plotted is without the deicing system, so the oscillations have nothing to do with deicing. By observing the temperatures and wind speeds at the same time one might determine if these oscillations are due to frequent shedding and rapid ice buildup. Another cause for these oscillations is that the model stops the turbine when the blade icing load reaches a certain threshold. That is when the icing loss is at 100%, but it then again tries to start the turbine after some time before stopping again. These hypotheses could be further investigated by comparing the icing loss with blade icing load, icing rate, wind speed and temperature at the same time. Unfortunately, there was not enough time to investigate this further for this work, but it is brought to attention for future research projects to investigate this behavior more deeply to understand what is causing the behavior and how large effect it has on the icing loss forecasts.

The icing losses from April are shown in Figure 4-9 (d) with the corresponding production time series shown in Figure 4-10. It shows a major icing episode in mid-April where all models give a significant icing loss up to 100%. From Figure 4-9 (d) this icing episode appears to occur at the same time for all models. This major icing episode in Figure 4-9 (d) from 11th of April to 17th of April are also zoomed in on and plotted in Figure 4-9 (e). Here it becomes more apparent that the icing episode does not arise at the same time for all models. Both KVT Meso hindcast and KVT Meso forecast the icing loss seem to occur slightly before the MEPS forecasts and increase sooner than MEPS. During the episode however, there are large hourly variations between the different models during the episode. And all models show this oscillating behavior between 100% icing loss and 0% icing loss, making it hard to determine if there is a time displacement between the models. However, the icing episode ends around 17th of April. For KVT Meso hindcast and KVT Meso forecast, the icing loss ends at the exact same time, while the end of the icing episode for the MEPS models differs with some hours before and after the KVT Meso simulations.

4.3.2 Relationship Between Power Productions

The following plot is of the three different production time series that IceLoss2.0 provide. One is the potential production, that is the production not influenced by icing or other curtailments. This is solely dependent on the wind speed from the numerical weather prediction model used as input. The second production time series is the production with icing. This is not the production only when icing occurs, but rather the potential production that is adjusted down when icing occurs. Finally, the last time series is the production with deicing. Here there is a possibility of icing, as for the production with ice, but the deicing module is also activated. If there is no icing, all these production timeseries would be identical, as is the case for 9th of April in Figure 4-10.

 Figure 4-10 of the production time series also provides a shaded blue area to mark icing episodes from the blade cylinder model, and a black shaded area underneath the production time series to show when deicing occurs.
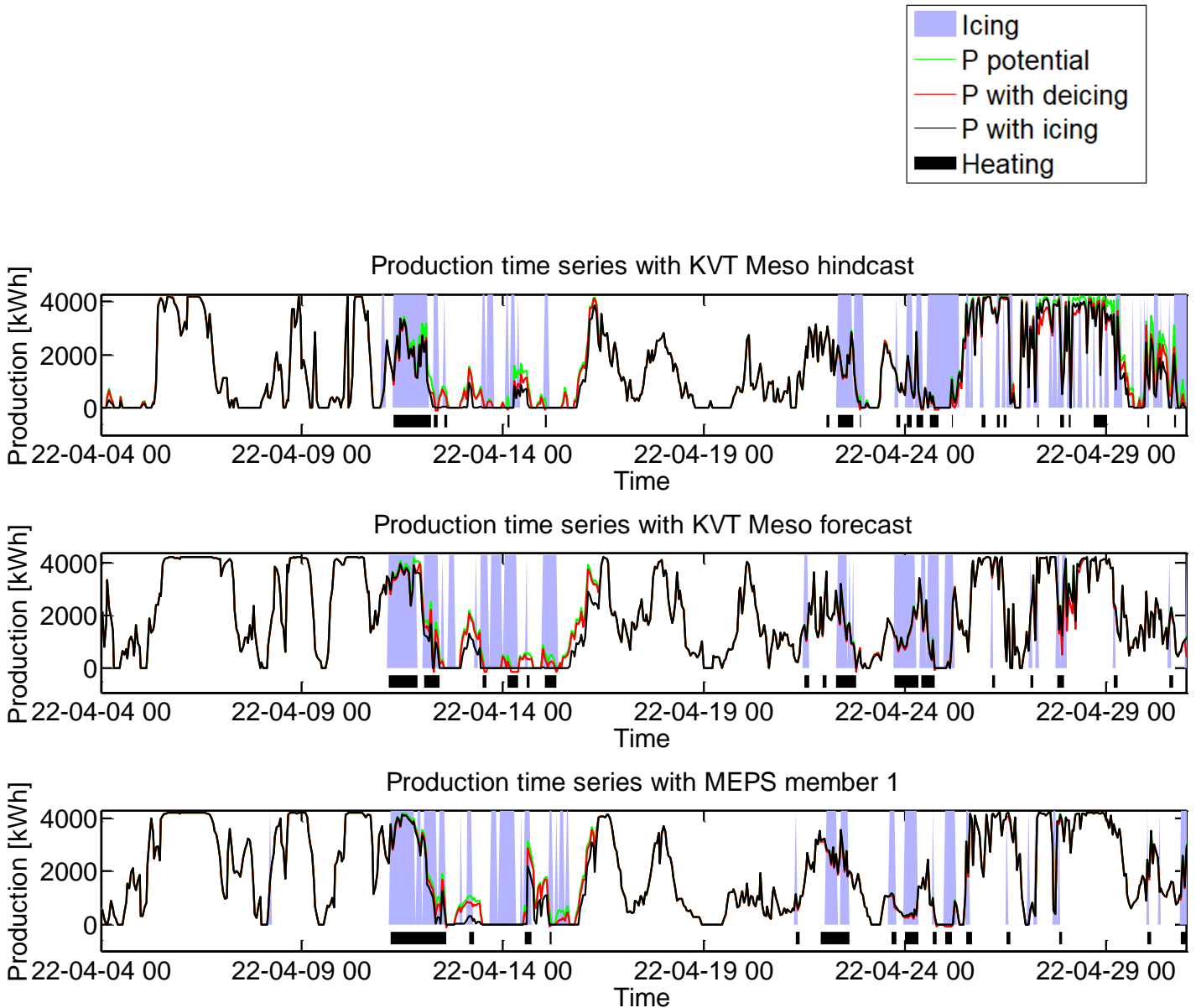
Figure 4-10: Production time series over April 2022 from IceLoss2.0 with the three different NWPs as input. Potential production marked in green, production with deicing in red and production with ice in black. The shaded blue areas marked episodes of icing and the thick black lines represents times when the deicing module is activated.

Firstly, Figure 4-10 show that during the first week of the April time series there is no icing. All production (potential, with icing, and with deicing) time series align and appear as one uniform line. Figure 4-9 (e) confirms also confirms this. Additionally, spikes with high production seem to appear at the same time for all three IceLoss2.0 simulations within this first week. Nevertheless, there are some variations in length and magnitude of these spikes. Both KVT Meso forecast and MEPS member 1 seem to have longer episodes with high production than KVT Meso hindcast, again this shows why the total production numbers were lower for KVT Meso hindcast.

Another interesting result that Figure 4-10 demonstrates, is that the icing episode occurring around the 13th of April begins at the exact same time for all three simulations. Since the timing is so similar for all three NWP models, it implies that none of the models have an extraordinary advantage in terms of timing the icing events. However, Figure 4-9 (e) of the icing losses during this episode show major variations between the three models at an hourly resolution. It would be an interesting next step to investigate if this correlates with the actual icing episodes from SCADA data.

At the very end of the time series plots in Figure 4-10, from 26th of April, KVT Meso hindcast has detected a quite heavy icing episode where KVT Meso forecast and MEPS have not. KVT Meso forecast only shows small icing episode around the 27th or 28th, but the losses here are very small. MEPS also show an even smaller episode with almost no loss during this day. KVT Meso hindcast are definitely more sensitive to icing than the other two models as it picks up this icing episode while other models do not.

The icing for KVT Meso hindcast also shows an 'on and off' behavior at the end of the time series in Figure 4-10, and the production with ice curve also have this oscillating behavior where the production drops instantaneously and then jump rapidly up again. The potential production at this moment is almost at full capacity, suggesting that during this icing episode there are strong winds. As the rotational speed of the blade increases, the centrifugal force also increases, leading the blade ice load to shed more easily. This might be what happens when production increases rapidly. However, if this is the case, there must also be a very high icing rate for production to drop so suddenly as well.

4.4 Validity of Results

The total icing losses and production numbers are highly influenced by the number of missing data from the MEPS model. This makes it more difficult to determine whether the low icing losses are due to the fact that the model underestimates icing, or if it is because long periods of data is missing where icing could have occurred. Probably, when looking at a snippet of the production time series from April 2022 in Figure 4-10, it is a combination of both. To get a clearer picture of how well the MEPS data works with IceLoss2.0, more data is needed. Preferably from a longer time frame over several winters.

Not only are there days when the data is missing altogether, but there are also several days where the closest simulation to the forecasting date where missing, and previous simulations

were used to retrieve a forecast for that day. It is known that for forecasting models, the uncertainty of the forecast increases with lead time (Ingvaldsen et al., 2022). Therefore, for some days the uncertainty might be much higher than for the days where the closest possible forecast was available.

The relationship between the wind speeds and the production numbers are determined by the turbine power curve. To include icing, a reduction matrix is used to describe the relationship between modelled icing load and the production loss. However, this reduction matrix was tuned by comparing icing losses between SCADA data and the original IceLoss2.0 model with historical WRF simulations as input. In fact, each input model type should have had its own reduction matrix which is tuned by their respective icing losses up against the SCADA database. This would increase the trustworthiness of the results from the forecasting simulations. It is apparent that this has influenced the resulting icing losses, but it is difficult to determine the gravity of this change. Therefore, the uncertainty in icing losses from IceLoss2.0 with MEPS and KVT Meso forecast is much higher than for IceLoss2.0 with KVT Meso hindcast.

5 Further Work

As the objective of this work was to investigate if the IceLoss2.0 modes was possible to be used with forecasting data such as MEPS and KVT Meso forecast, several simplifications were made. The first one being adding the forecasts together into a continuous time series. To simulate one forecast at a time, an implementation where the blade ice load is corrected with real measurements, SCADA data, is needed. This is to avoid every forecast starting with no ice on the blade. By creating one continuous time series of several forecasts, the icing load is only transmitted from one forecast and into the next. Although it is possible to extract this icing load from the previous forecast when simulation one at a time, it would be better to adjust from SCADA data to avoid model errors accumulating.

The next step should be to tune the power reduction matrix for MEPS data, and maybe KVT Meso forecast as well, although it might not be necessary due to time similarity of these models. The power reduction matrix was originally made by tuning the icing losses with KVT Meso hindcast. Maybe the differences in icing loss between KVT Meso and MEPS could be adjusted only by tuning this matrix.

The model also needs to be validated with SCADA data to confirm which input model provides the closest result both in magnitude and timing of the icing loss.

It is preferable to include both MEPS and KVT Meso forecast when further developing the IceLoss2.0 model due to its statistical advantages. Especially due to the risk of missing forecasts. That way the two datasets can also work as backup when the other one is missing.

In this work, MEPS model simulations with the ICE3 microphysics scheme were used. However, this scheme has proven to underestimate the supercooled liquid water content. That is, when temperatures drop below 0 degrees the liquid water is transferred into ice too quickly (B. J. K. Engdahl et al., 2020). The QQ plots of the water vapor in Figure 4-7 also show that the water content from MEPS is lower than for KVT Meso hindcast and KVT Meso forecast. A study by Engdal et. al. (B. J. K. Engdahl et al., 2020) constructed a new microphysics scheme for the HARMONIE-AROME model based on the Thompson physics scheme as this has proven to produce the best supercooled liquid water content representation (Nygaard et al., 2011). This new scheme, called ICE-T gives higher amounts of supercooled liquid water (B. Engdahl et al., 2020). Waiting for an update of the MEPS model with this new

microphysics scheme could therefore be of interest to increase the icing losses from IceLoss2.0 with MEPS.

6 Conclusions

This work has shown that using forecasting data like KVT Meso forecast and MEPS is possible with simplified methods such as creating a uniform time series of all forecasted dates and assuming that the ice load from one forecast follows into the next.

By the small differences in icing loss between the three models, it shown that the model has potential to be used for icing loss forecasting needs, with some small adjustments. The lack of MEPS data has been a challenge during this work, and the short timeframe of the datasets makes it hard to prove the differences between the models. According to the icing losses where the missing dates were filtered out, the MEPS model provided the lowest icing losses. This statement is confirmed further by studying the icing loss time series. This may be due to the ICE3 microphysics scheme that is used in the MEPS simulations, which underestimated the amount of supercooled liquid water.

When it comes to time accuracy of the icing events, all models seem to correlate well when looking at the day to day icing. But there are large differences between the models at an hourly rate. The icing losses also fluctuate a lot during an icing episode, making it more difficult to investigate the icing loss time series and determine if there are any time shifts between the models. The reason for this is unknown, although a hypothesis about it being due to ice shedding has been presented.

Both MEPS and KVT Meso forecast provided higher wind speeds, in turn leading to higher power production numbers. This should also be tested against SCADA to see what production amount is the most accurate.

Finally, this work has successfully implemented WRF forecast and MEPS into IceLoss2.0 for one turbine in the Kvitfjell/Raudfjell wind farm and yielded comparable results to WRF hindcast. The results are promising for IceLoss2.0 to be used for icing loss forecasting using both WRF and MEPS.

Appendix

Ensemble member	Additional missing dates	Total amount of missing dates from winter timeseries
1	11.11.21	11.5%
2	09.12.21	11.5%
3	09.12.21, 28.95.22	11.8%
4	none	11.0%
5	none	11.0%
6	09.12.21	11.5%
7	09.12.21	11.5%
8	none	11.0%
9	11.11.21	11.5%
10	16.09.21, 29.09.21, 30.09.21, 03.11.21, 11.11.21, 09.12.21, 13.12.21, 01.01.22, 02.01.22, 03.02.22, 12.03.22, 23.04.22, 06.05.22, 09.05.22, 11.05.22, 12.05.22, 14.05.22, 16.05.22, 17.05.22, 25.05.22	18.7%
11	29.09.21, 30.09.21, 11.03.22	12.2%
12	29.09.21	11.5%
13	09.12.21	11.5%
14	none	11.0%
15	11.11.21	11.5%
16	12.03.22	11.5%
17	12.03.22	11.5%
18	13.12.21, 11.03.22, 12.03.22	12.2%
19	10.12.21, 01.01.22, 02.01.22, 03.01.22	12.6%
20	10.12.21, 01.01.22, 02.01.22, 03.01.22	12.6%
21	03.11.22, 10.02.22	11.8%
22	03.11.22, 10.02.22	11.8%
23	01.01.22, 02.01.22, 03.01.22	12.2%
24	03.11.21	11.5%
25	29.09.21, 12.03.22	11.8%
26	01.01.22, 02.01.22, 03.01.22	12.2%
27	16.09.21, 29.09.21, 03.11.21	12.2%
28	12.03.22	11.5%
29	10.12.21, 01.01.22, 02.01.22, 03.01.22	12.6%
30	03.11.21	11.5%

Bibliography

Ahrens, C. D., & Henson, R. (2020). *Meteorology Today* (13th ed.). Cencage.

Andersen, R. B. (2022). *Validation of IceLoss2.0 model for Icing on Wind Turbines*.

Byrkjedal, Ø. (2022). In.

Clausen, N. E. (2017). *IceWind final scientific report: Improved forecast of wind, wave and icing*.

Engdahl, B., Nygaard, B. E., Losnedal, V., Thompson, G., & Bengston, L. (2020). Effects of the ICE-T microphysics scheme in HARMONIE-AROME on estimated ice loads on transmission lines. *Cold Regions Science and Technology*, *179*. https://doi.org/https://doi.org/10.1016/j.coldregions.2020.103139.

Engdahl, B. J. K., Thompson, G., & Bengtsson, L. (2020). Improving the representation of supercooled liquid water in the HARMONIE-AROME weather forecast model. *Tellus A: Dynamic Meteorology and Oceanography*, *72*(1), 1-18. https://doi.org/10.1080/16000870.2019.1697603

Ferrieira, P. F. (2016). *Volume and Price in The Nordic Balancing Power Market* Norwegian University of Science and Technology]. http://hdl.handle.net/11250/2404699

Forgner, I.-L., Singleton, A. T., Køltzow, M. Ø., & Andrae, U. (2019). Convection-permitting ensembles: Challenges related to their design and use. *Q J R Meteorol Soc*, *145*(S1), 90– 106. https://doi.org/https://doi.org/10.1002/qj.3525

Frogner, I.-L., Andrae, U., Bojarova, J., Callado, A., Escribà, P., Feddersen, H., Hally, A., Kauhanen, J., Randriamampianina, R., Singleton, A., Smet, G., van der Veen, S., & Vignes, O. (2019). HarmonEPS—The HARMONIE Ensemble Prediction System. *Weather and Forecasting*, *34*(6), 1909-1937. https://doi.org/https://doi.org/10.1175/WAF-D-19-0030.1

Gebrekiros, Y., & Doorman, G. (2014, 27-31 July 2014). *Balancing energy market integration in Northern Europe — Modeling and case study* PES General Meeting | Conference & Exposition, National Harbor, MD, USA.

Hong, S.-Y., Noh, T., & Dudhia, J. (2006). A New Vertical Diffusion Package with an Explicit Treatment of Entrainment Processes. *Monthly Weather Review*, *134*(9), 2318–2341. https://doi.org/https://doi.org/10.1175/MWR3199.1

Ingvaldsen, K., Molinder, J., & Grini, S. (2022, June 19-23 2022). *Combining Ensemble Icing Forecasts with Real Time Measurements for Power Line and Wind Turbine Applications* IWAIS 2022 - Int. Workshop on Atmospheric Icing of Structures, Montreal, Canada.

ISO12494. (2017). *Atmospheric icing of structures*

Jan, D. (2021). *The Difference Between Deterministic and Ensemble Forecasts*. Retrieved 19th May 2023 from https://www.worldclimateservice.com/2021/10/12/difference-between-deterministic-and-ensemble-forecasts/

Kjeller Vindteknikk. (n.d.-a). *"Appendix A - KVT IceLoss [SWE06]*.

Kjeller Vindteknikk. (n.d.-b). *KVTMeso - WRF Simulations*.

Kurppa, M., Rissanen, S., Byrkedal, Ø., & Lehtomäki, V. (2022). *Validation of day-ahead icing loss forecasts with SCADA data* Winterwind Skellefteå. https://windren.se/WW2022/02_1_04_Kurppa_Validation_of_icing_loss_forecasts_with_SCADA_data_Pub_v1.pdf

Lamraoui, F., Fortin, G., Benoit, R., & Masson, C. (2014). Atmospheric icing impact on wind turbine production. *Cold Regions Science and Technology*, *100*(0165-232X), 36-49. https://doi.org/https://doi.org/10.1016/j.coldregions.2013.12.008

Le Moigne, P. (2009). *SURFEX Scientific documentation*.

Lehtomäki, V. (2022). *Analysis: Large-scale icing events in Finland during November 2022*. Retrieved 30th of May 2022 from https://www.vindteknikk.com/news/analysis-large-scale-icing-events-in-finland-during-november-2022/

Liléo, S., Berge, E., Undheim, O., Klinkert, R., & Bredesen, R. E. (2013). Long-term correction of wind measurements *Elforsk report 13:18*. https://energiforskmedia.blob.core.windows.net/media/19814/long-term-correction-of-wind-measurements-elforskrapport-2013-18.pdf

Lindvall, J. (2017). *IceLoss2.0 -detailed calculations of ice loads and the associated production losses on wind turbines*. Energimyndigheten.

MetOffice. (n.d.). *What is an ensemble forecast?* Retrieved 31st of May 2022 from https://www.metoffice.gov.uk/research/weather/ensemble-forecasting/what-is-an-ensemble-forecast

Molinder, J. (2021). *Forecasting of Icing Related Wind Energy Production Losses* Uppsala Universitet].

NCAR. (2023). *Weather Research & Forecasting Model (WRF)*. Retrieved 27.april from https://www.mmm.ucar.edu/models/wrf

Nilsen, P. T. F. (2019). *Wind turbines and ice breaking* UiT The Arctic University in Norway]. UiT. https://munin.uit.no/handle/10037/18093

NordPool. (n.d.). *Day-ahead market*. Retrieved 31st of May 2022 from https://www.nordpoolgroup.com/en/the-power-market/Day-ahead-market/

NVE. (2022a). *Hvordan fungerer kraftmarkedet?* Retrieved 31st of May 2022 from https://www.nve.no/reguleringsmyndigheten/slik-fungerer-kraftsystemet/hvordan-fungerer-kraftmarkedet/

NVE. (2022b). *I kraftsystemet handler mye om fysikk*. Retrieved 31st of May 2022 from https://www.nve.no/reguleringsmyndigheten/slik-fungerer-kraftsystemet/i-kraftsystemet-handler-mye-om-fysikk/

Nygaard, B. E., Kristjánsson, J. E., & Makkonen, L. (2011). Prediction of In-Cloud Icing Conditions at Ground Level Using the WRF Model. *Journal of Applied Meteorology and Climatology*, *50*(12), 2445–2459. https://doi.org/https://doi.org/10.1175/JAMC-D-11-054.1

Rissanen, S. (2023). *Experiences with IPS icing losses and Iceloss 2.2* WinterWind

Ronsten, G., Wallenius, T., Hulkkonen, M., Baring-Gould, I., Cattin, R., Durstewitz, M., Krenn, A., Laakso, T., Lacroix, A., Tallhaug, L., & others. (2012}). State-of-the-art of Wind Energy in Cold Climates. *IEA Wind Task XIX, VTT, Finland*.

Taufour, M., Vié, B., Augros, C., Delanoë, J., Delautier, G., Ducrocq, V., Lac, C., Pinty, J.-P., & Schwarzenböck, A. (2019). Evaluation of the two-moment scheme LIMA based on microphysical observations from the HyMeX campaign. *Quarterly Journal of the Royal Meterological Society*, *144*(714), 1398-1414. https://doi.org/https://doi.org/10.1002/qj.3283

Thompson, G., Rasmussen, R. M., & Manning, K. (2004). Explicit Forecasts of Winter Precipitation Using an Improved Bulk Microphysics Scheme. Part I: Description and Sensitivity Analysis. *Monthly Weather Review*, *132*(2), 519 - 542. https://doi.org/https://doi.org/10.1175/1520-0493(2004)132%3C0519:EFOWPU%3E2.0.CO;2

Wallenius, T., & Lehtomäki, V. (2015). Overview of cold climate wind energy: challenges, solutions, and future needs. *WIREs Energy and Environment*, *5*(2). https://doi.org/https://doi.org/10.1002/wene.170

Warpole, R. E., Myers, R. H., Myers, S. L., & Ye, K. (2014). *Probability and Statistics for Engineers and Scientists* (Ninth ed.). Pearson Education, Inc.